Title: Temporal analysis of enhancers during mouse brain development reveals dynamic regulatory function and identifies novel regulators of cerebellar development.

Authors: Miguel Ramirez[1,2], Yuliya Badayeva[1,2], Joanna Yeung[1,2], Joshua Wu[1,2], Erin Yang[1,2], FANTOM 5 Consortium[3], Brett Trost[4], Stephen W. Scherer[4], Daniel Goldowitz[1,2]*

Author Affiliations: 1. Centre for Molecular Medicine and Therapeutics, BC Children's Hospital Research Institute, Vancouver, BC, Canada V6H 3V5; 2. University of British Columbia, Vancouver, BC, Canada V6T 1Z4; 3. RIKEN, 2-1 Hirosawa, Wako, Saitama 351-0198, Japan; 4. The Centre for Applied Genomics, The Hospital for Sick Children, Toronto, ON, Canada M5G 0A4

Corresponding Author: Daniel Goldowitz, Centre for Molecular Medicine and Therapeutics, BC Children's Hospital Research Institute, 950 W 28th Ave, Vancouver, BC, Canada V6H 3V5

Classification: Biological Sciences, Developmental Biology

Keywords: Enhancers, Brain development, Gene expression regulation, Epigenetics, Transcription factors, Mouse, Autism Spectrum Disorder

1 **Abstract**

2   In this study, we identified active enhancers in the mouse cerebellum at embryonic and

3 postnatal stages establishing the first catalog of enhancers active during embryonic cerebellum

4 development. The majority of cerebellar enhancers have dynamic activity between embryonic

5 and postnatal development. Cerebellar enhancers were enriched for neural transcription factor

6 binding sites with temporally specific expression. Putative gene targets displayed spatially

7 restricted expression patterns, indicating cell-type specific expression regulation. Functional

8 analysis of target genes indicated that enhancers regulate processes spanning several

9 developmental epochs such as specification, differentiation and maturation. We use these

10 analyses to discover one novel regulator and one novel marker of cerebellar development:

11 Bhlhe22 and Pax3, respectively. We identified an enrichment of *de novo* mutations and variants

12 associated with autism spectrum disorder in cerebellar enhancers. Our study provides insight into

13 the dynamics of gene expression regulation by enhancers in the developing brain and delivers a

14 rich resource of novel gene-enhancer associations providing a basis for future in-depth studies in

15 the cerebellum.

16

17 **Introduction**

18   Neuronal development is a complex and dynamic process that involves the coordinated

19 generation and maturation of countless cell types. For the most numerous neuron in the brain, the

20 cerebellar granule cell, neuronal differentiation consists of several steps beginning with the

21 commitment of neural stem cells to become specified neural precursors, followed by multiple

22 migratory stages to reach and mature at its final destination (Consalez, Goldowitz, Casoni, &

23 Hawkes, 2021). Underpinning these events is the expression of gene regulatory networks that

24 drive dynamic molecular processes required for proper brain formation (Ziats, Grosvenor, &

25 Rennert, 2015). However, the transcriptional mechanisms that precisely regulate these gene

26 expression programs have not been fully described.

27   Gene expression is typically activated when transcription factors (TFs) bind to non-

28 coding regulatory elements and recruit the necessary components to begin transcription. Among

29 the several classes of non-coding sequences that regulate gene expression, enhancers are the

30 most common, with thousands predicted to coordinate transcriptional regulation during

31 development (Heinz, Sven, Romanoski, Benner, & Glass, 2015). Enhancers are stretches of DNA

32   that bind to TFs and upregulate distal target gene expression. In the brain, enhancers help to

33   ensure that gene expression is spatially- and temporally-specific, defining what genes will be

34   active during distinct stages of development (Nord & West, 2020). Transcriptional regulation by

35   enhancers has been shown to be critical for cellular identity, maturation during central nervous

36   system (CNS) development, and activity-dependent responses in mature neurons (Frank et al.,

37   2015; Pattabiraman et al., 2014). A detailed understanding of the enhancers that govern changes in

38   gene expression during embryonic and early postnatal brain development remains limited.

39   Profiling genome-wide enhancer activity at different time points and identifying their gene

40   regulatory targets can provide insight into developmental processes regulated by enhancer

41   elements.

42   Several molecular properties have been associated with enhancer activity, and the

43   advancement of sequencing technology has facilitated their identification genome-wide in

44   several developing brain structures (Carullo & Day, 2019). Enhancers are marked with histone

45   post-translational modifications H3K4me1 and H3K27ac, both of which contribute to opening

46   chromatin for TF binding (Calo & Wysocka, 2013). H3K27ac delineates active from poised

47   elements, and has been a reliable marker for enhancer activity genome-wide (Creyghton et al.,

48   2010). Analysis of these marks, in conjunction with transcriptomic and epigenomic datasets, has

49   revealed that the vast majority of non-coding variants associated with neurological and

50   psychiatric disorders are found within these regulatory elements, highlighting their importance in

51   functional readout in the brain (Barešić, Nash, Dahoun, Howes, & Lenhard, 2020). Thus, profiling

52   enhancer-associated histone modifications in the brain across time provides a comprehensive

53   understanding of gene-regulatory principles, disease-associated variants, and the genetics of

54   brain development (Nott et al., 2019).

55   The cerebellum has been a long-standing model to study the developmental genetics of

56   the brain. This is, in part, due to the limited number of cell types, well-defined epochs of

57   development for these cell types and a simple trilaminar structure in which these cells are

58   organized, making for an enhanced resolution of events in time and space (Wang, V. Y. & Zoghbi,

59   2001). More recently, the study of cerebellar development has gained added interest through its

60   documented role in the etiology of ASD (Stoodley & Limperopoulos, 2016). Previously, we

61   developed a 12-timepoint transcriptional analysis of the developing cerebellum leading to the

62   discovery of novel TFs critical for proper development (Zhang, P. G. Y. et al., 2018). More

63   recently, the developing cerebellum has served as an ideal setting for pioneering single-cell

64   RNA-seq time course studies (Carter et al., 2018; Peng et al., 2019; Wizeman, Guo, Wilion, & Li,

65   2019). At the level of gene expression regulation, chromatin accessibility and enhancer activity

66   have been examined previously in the postnatal cerebellum, leading to the discovery of distinct

67   transcriptional profiles between immature and mature neurons, coordinated by non-coding *cis*-

68   regulatory sequences (Frank et al., 2015). However, a comprehensive atlas of enhancers defining

69   the role they play during embryonic and early postnatal cerebellar development has yet to be

70   established. Profiling these non-coding regulatory elements and their target genes will discover

71   novel genetic drivers of the precisely-timed and cell-specific molecular events in the developing

72   cerebellum.

73   We utilize chromatin immunoprecipitation followed by sequencing (ChIP-seq) of

74   enhancer associated histone marks H3K4me1 and H3K27ac at 3 stages of embryonic and early

75   postnatal cerebellar development. We identify temporally specific enhancers using a differential

76   peak analysis comparing postnatal and embryonic timepoints.   Transcription factor motif

77   enrichment and prediction of gene targets led to the elucidation of molecular processes regulated

78   by enhancers during these stages. We use these analyses to discover two novel regulators of

79   cerebellar development, Pax3 and Bhlhe22: a novel marker of GABAergic progenitors and a

80   regulator of postnatal granule cell migration, respectively. Finally, we identify an enrichment of

81   autism spectrum disorder (ASD) associated SNPs and *de novo* variants found in ASD-affected

82   individuals in cerebellar enhancers, functionally annotating ASD-associated variation. Our study

83   provides further insight into the dynamics of gene expression regulation by enhancers in the

84   developing brain and delivers a rich resource to help understand the developmental and

85   functional genetics of the developing cerebellum.

86

87   **Results**

88   **Enhancer identification during cerebellar development**

89   To identify enhancers active during embryonic and postnatal cerebellar development, we

90   generated genome-wide H3K27ac and H3K4me1 ChIP-seq profiles from mouse cerebella

91   dissected at embryonic day 12 (E12), postnatal day 0 (P0) and postnatal day 9 (P9) (**Figure 1A**).

92   These developmental days represent 3 distinct stages of murine cerebellar development, each

93   with its own developmental profile (Goldowitz & Hamre, 1998). H3K27ac and H3K4me1 signals

94   were reproducible between biological replicates as exemplified in a region on chromosome 14

95   (**Figure 1B**). There was a high correlation between replicates for both marks at each age

96   (**Supplementary Figure 1A**). Therefore, we had confidence in using our H3K27ac and

97   H3K4me1 data in downstream analyses. Robust cerebellar enhancers were identified by the

98   presence of overlapping peaks between the two enhancer-associated histone marks at each age.

99   This highlighted a total of 9,622 peaks; 5,859, 474, and 3,289 peaks that were in both the

100   H3K27ac and H3K4me1 datasets at E12, P0, and P9, respectively (**Figure 1C**). Duplicate peaks

101   between ages were removed, producing a list of **7,024** active cerebellar enhancers derived from

102   overlapping H3K27ac and H3K4me1 signals (Supplementary Data 1).
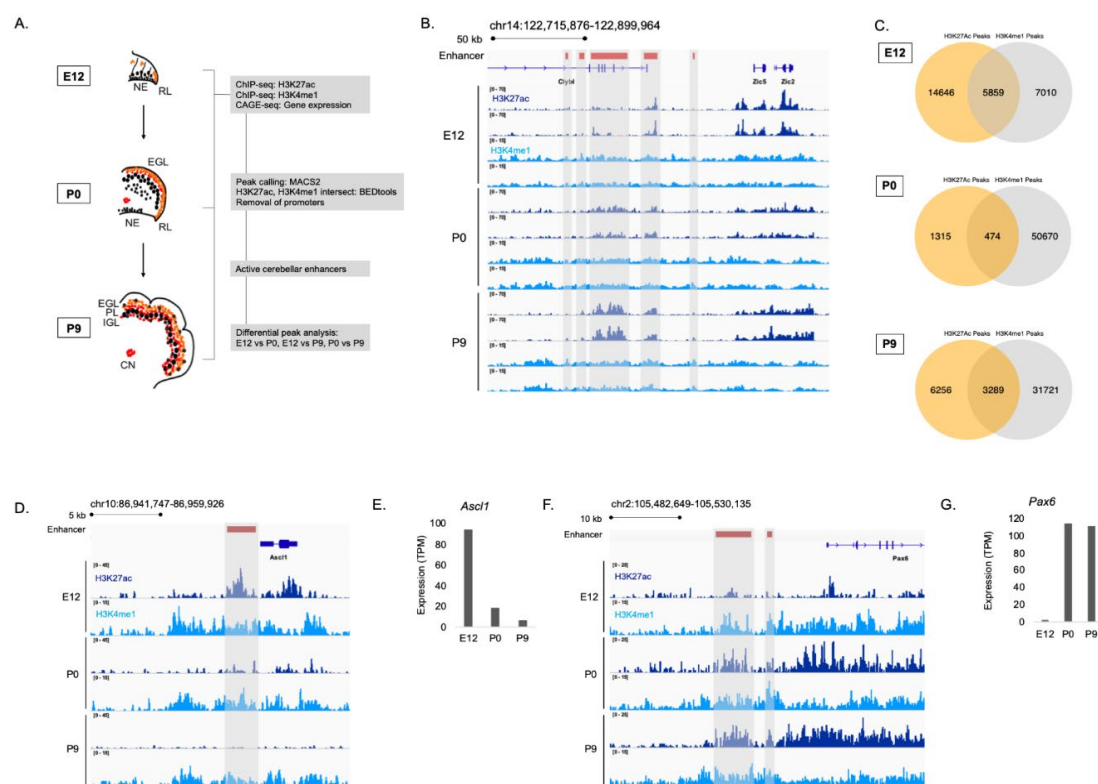
103

104

105   **Figure 1. Enhancer identification during cerebellar development. A)** An overview of the stages of cerebellar
106   development profiled in this study. The datasets collected at these ages and the downstream analyses are shown.
107   Labels: NE: Neuroepithelium, RL: Rhombic lip, EGL: External granular layer, PL: Purkinje layer, IGL: Inner
108   granular layer, CN: Cerebellar nuclei **B)** A region of the mouse genome chr14:122,715,876-122,899,964 (mm9) in
109   the Integrative Genomics Viewer (IGV) showing H3K27ac and H3K4me1 profiles across biological replicates of
110   E12, P0, P9 cerebella. Active cerebellar enhancers are highlighted (gray box). **C)** Venn diagrams displaying overlap
111   between H3K27ac and H3K4me1 peaks at each E12, P0 and P9. **D-E)** An example of a cerebellar enhancer
112   identified from the E12 cerebella. Shown is normalized H3K27ac and H3K4me1 signal at the enhancer (gray box),
113   as well as **(E)** normalized CAGE-seq expression of the nearest gene, *Ascl1*, across developmental time, at E12, P0,
114   P9. TPM, Transcripts Per Million. **(F-G)** An example of a cerebellar enhancer identified from the P9 cerebella.
115   Shown is normalized H3K27ac and H3K4me1 signal at the enhancer (gray box), as well as **(G)** normalized (TPM)
116   CAGE-seq expression of the nearest gene, *Pax6*, across developmental time, at E12, P0, P9.

117   The relationship between enhancer activity and genes relevant to cerebellar development

118   is shown in genomic regions flanking *Ascl1* and *Pax6,* two genes critical to cerebellar

119   development (Kim, Battiste, Nakagawa, & Johnson, 2008; Yeung, Ha, Swanson, & Goldowitz, 2016b).

120   We identified an enhancer active at E12 located in close proximity to *Ascl1* (**Figure 1D**). A

121   decrease in the H3K27ac ChIP-seq signal at this enhancer corresponded to a decrease in *Ascl1*

122   gene expression (**Figure 1E**). We identified two active enhancers at P9 located near *Pax*6

123   (**Figure 1F**). H3K27ac ChIP-seq signal also showed a pattern of activity similar to *Pax6*

124   expression, increasing from embryonic to postnatal ages (**Figure 1G**). These results provide

125   validation for the enhancers identified in our dataset in regulating genes critical to cerebellar

126   development.

127   We compared our list of robust cerebellar enhancers to three previously published

128   enhancer datasets. First, P7 H3K27ac ChIP-seq and DNase-seq profiles previously generated by

129   Frank et al (2015) were compared to robust cerebellar enhancers. Greater than 90% of our

130   reported cerebellar enhancers are replicated by H3K27ac and DNAse-seq peaks from this study

131   (**Supplementary Figure 1B-C**). Second, enhancers retrieved from the enhancer database

132   EnhancerAtlas 2.0, reporting enhancer activity in the mouse cerebellum at P0-P14 (Gao & Qian,

133   2020), were compared to robust cerebellar enhancers were compared to. We found that 73%, and

134   80% of our enhancers overlapped with the postnatal cerebellum enhancer dataset at P0, and P9,

135   respectively (**Supplementary Figure 1D**). Third, mouse enhancers that had experimentally

136   validated hindbrain activity at E11.5 from the VISTA Enhancer Browser (Visel, Minovitsky,

137   Dubchak, & Pennacchio, 2007) were compared to cerebellar enhancers. We found that 56% of

138   VISTA enhancers overlap with our cerebellar enhancer sequences at E12 (**Supplementary**

139   **Figure 1E**). These confirmative findings indicate our approach was effective in capturing active

140   cerebellar enhancers.

141

142   **Enhancer dynamics during cerebellar development**

143   The dynamics of enhancer activity over cerebellar development were examined through a

144   differential peak analysis of H3K27ac signal. The majority, **89% (6238/7023),** of cerebellar

145   enhancers had significant differences in peak signal (adjusted p-value $\leq$ 0.05) throughout

146   cerebellar development (**Figure 2A**). At P9, **1273** cerebellar enhancers were significantly active

147   compared to either P0 or E12 (Supplementary Data 2). At E12, **4432** active enhancers were

148 differentially active compared to either P9 or P0 (Supplementary Data 2). At P0, in contrast, only

149 a small number of enhancers with differential signal was identified (403 and 154 showed

150 significant changes when compared to E12 and P9, respectively). However, none of these P0

151 cerebellar enhancers were differentially active when compared to both E12 and P9, indicating

152 that enhancer activity did not spike at birth. Taken together, this analysis highlights two

153 temporally specific windows of enhancer activity at Early (embryonic) and Late (postnatal)

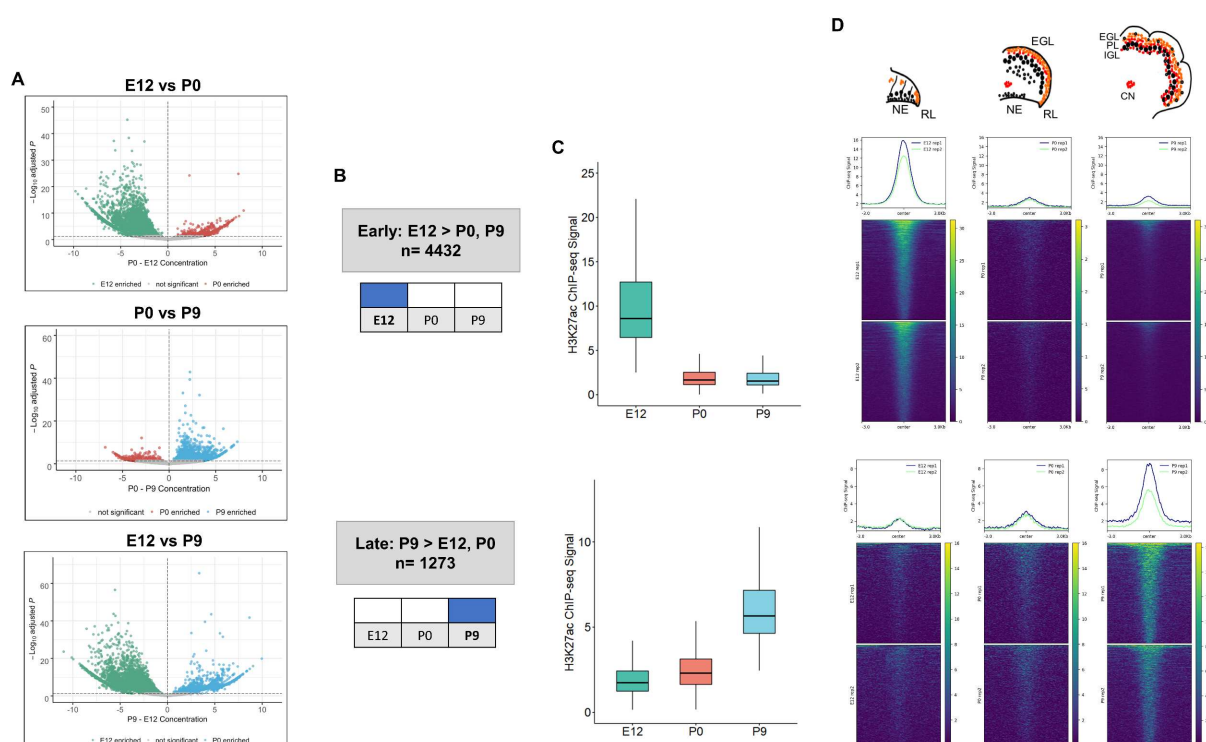154 stages (**Figure 2B).**

155

156 **Figure 2. Enhancer activity is dynamic throughout cerebellar development. A)** Volcano plots showing robust
157 cerebellar enhancers with differential H3K27ac peak signal for three comparisons: E12 vs P9, E12 vs P0, and P0 vs
158 P9. Differential signal strength was identified for 4433 and 4355 robust cerebellar enhancers when comparing E12
159 to P9 and to P0, respectively. At P9, 1275 and 403 robust cerebellar enhancers had differential signal when
160 compared to E12 and P0, respectively. Enhancers with significant differential activity are colored at a cutoff of an
161 adjusted p-value < 0.05. Displayed on the y-axis is the negative log10 adjusted p-value and on the x-axis is the
162 difference in ChIP-seq signal between to the ages for a given peak. **B)** A diagram displaying how Early and Late
163 active cerebellar enhancers were classified based on differential peak analysis results. **C)** A boxplot showing mean
164 ChIP-seq signal (y-axis) for all Early (upper) and Late (lower) active enhancers. Error bars represent the standard
165 error of the mean. **D)** Mean profile and heatmaps of H3K27ac signal at the midpoint of our predicted cerebellar
166 enhancers (rows ± 3kb) in Early and Late groups at E12, P0 and P9.

167
168
169 Distinct patterns of enhancer activity were observed for temporally classified enhancers.

170 For Early active enhancers, there was a loss of mean H3K27ac signal over time, with a steep

171 decline after E12 (**Figure 2C**). Late active enhancers exhibited a gain in activity over time, with

172 mean H3K27ac signal increasing steadily through development. These patterns are seen when

173 looking at the changes in signal flanking the summits of our peaks across time (**Figure 2D**).

174 These results indicate that the majority of cerebellar enhancers are dynamic throughout time and

175 exhibit temporally specific activity.

176

177 **Cerebellar enhancers are enriched for neural transcription factor binding sites in an age-**

178 **dependent manner**

179 We then sought to identify transcription factors whose activity is dictated by the

180 availability of robust cerebellar enhancers, as many neural lineage-defining factors drive cell

181 commitment in the developing brain through enhancer binding (Elsen et al., 2018; Lindtner et al.,

182 2019). We used HOMER to search for enriched motifs (adjusted p-value < 1E-11) in Late and

183 Early active cerebellar enhancers and then matched them to known transcription factor motifs in

184 the JASPAR database (Heinz, S. et al., 2010). This analysis revealed a distinct set of significantly

185 enriched motifs for Early and Late enhancers matching predicted TFs with both known and novel

186 regulatory roles in cerebellar development (**Figure 3A**). TFs enriched in the Early active

187 enhancers show a decrease in expression over time while TFs enriched in the Late active

188 enhancer group show an increase in expression over time. This correspondence between enriched

189 TF expression and enhancer activity provides validation for our findings and indicates the timing

190 of enhancer activity may be dictated by the expression and binding of these enriched TFs.

191 The top three enriched TF motifs for Early active enhancers were Ascl1, Meis2 and

192 Atoh1 (**Figure 3A**). These TFs have established roles in cerebellar development, acting as

193 markers of GABAergic or glutamatergic cell types and regulators of differentiation (Ben-Arie et

194 al., 1997; Kim et al., 2008; Wizeman et al., 2019). Importantly, many of the motifs enriched in the

195 Early group matched with TFs which have received little to no attention in the cerebellum,

196 including Sox4, Lhx2, Rfx4, Pou3f1 and Pax3 (**Figure 3A**). These TFs have been previously

197 associated with the development of other brain areas (Frantz, Bohner, Akers, & McConnell, 1994;

198 Porter et al., 1997; Su et al., 2016; Zhang, D. et al., 2006). In contrast, the TFs matching the motifs

199 enriched in the Late active enhancers have a previously identified role in cerebellar development;

200 but not necessarily involved in the same processes (**Figure 3A**). For example, the top 3 enriched

201 motifs matched with Neurod1, Nfia/b/x, and NF1, which have all been associated with granule

202 cell differentiation (Miyata, Maeda, & Lee, 1999; Sanchez-Ortiz et al., 2014; Wang, W. et al., 2007).

203 However, two other TFs with enriched binding sites, Pax6 and Smad4 have been found to be

204 critical for granule cell precursor proliferation, a process preceding differentiation (Swanson &

205 Goldowitz, 2011). These results suggest a dynamic role for the majority of our Early and Late

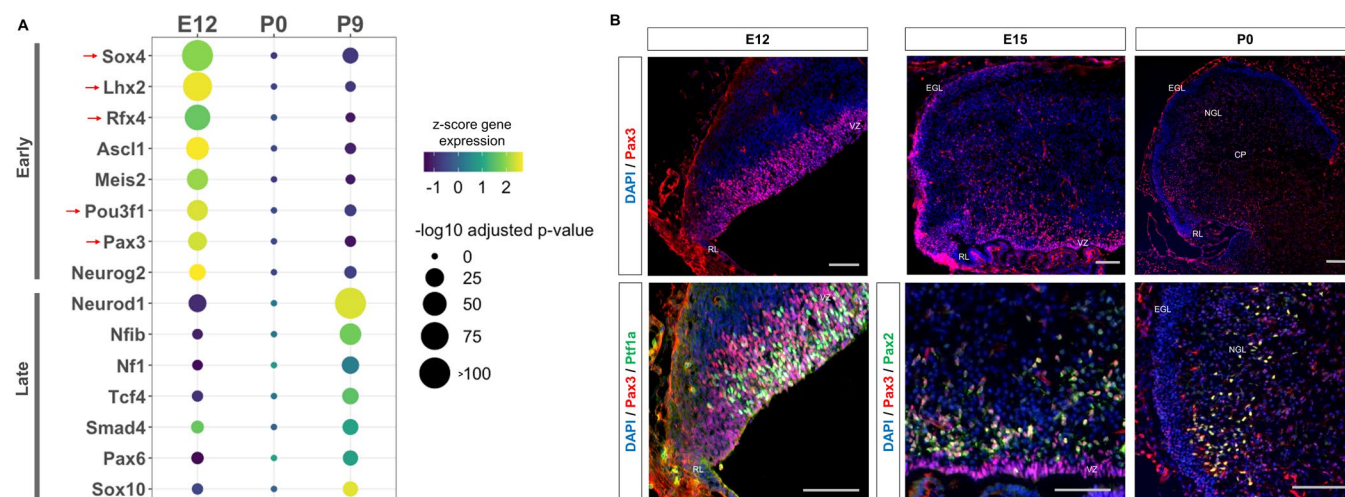206 active enhancers, driven by TFs involved in distinct stages of neuron development.

207

208
209 **Figure 3. Neural transcription factors with known and novel function in the developing cerebellum are**
210 **enriched in dynamic cerebellar enhancers. A)** Dot plot displaying significantly enriched (adjusted p-value < 1E-
211 11) motifs and the predicted matching transcription factor (TF). Displayed are the results for Early (top) and Late
212 (bottom) active enhancers. TFs with an unknown functional role in cerebellar development are indicated with a red
213 arrow. Size of the dots indicate the negative log10 adjusted p-value for a given motif and the color scale displays the
214 z-score normalized expression throughout the cerebellar developmental time course. **B**) Top: Immunofluorescent
215 staining of Pax3 in the mouse cerebellum at E12, E15 and P0. Bottom: Pax3 and Ptf1a immunofluorescent co-
216 staining of the E12 mouse cerebellum. Immunofluorescent co-staining of Pax3 and Pax2 in the mouse cerebellum at
217 E15 and P0. Labels: CP: Cerebellar parenchyma, EGL: External granular layer, NGL: Nascent granular layer, RL:
218 Rhombic lip, VZ: Ventricular zone, Scalebars = 100um.

219

220 **Early active enhancers are enriched for Pax3 binding sites, a novel marker for GABAergic**

221 **cells**

222 The TF motif enrichment analysis of Early enhancers led to the discovery of several TFs

223 with novel in the context of embryonic cerebellar development; potentially involved in seminal

224 aspects of development such as cellular specification or commitment. As a case study, we

225 focused on Pax3, as other members of the Pax protein family have been shown to play key roles

226 in the developing cerebellum (Leto et al., 2009; Urbánek, Fetka, Meisler, & Busslinger, 1997; Yeung,

227 Ha, Swanson, & Goldowitz, 2016a). Indeed, we observed robust expression in the ventricular zone

228 (VZ); a neural progenitor region for GABAergic cells in the cerebellum (Leto, Carletti, Williams,

229   Magrassi, & Rossi, 2006) (**Figure 3B**). Colocalization between Pax3 and Ptf1a, the GABAergic

230   lineage-defining molecule in the cerebellum (Hoshino et al., 2005), confirmed expression within

231   GABAergic neural progenitors. At E15, Pax3+ cells are seen in the region just dorsal to the VZ,

232   which consist of post-proliferative cells such as Purkinje cells and interneurons (Hoshino et al.,

233   2005; Leto et al., 2006) (**Figure 3B**). We examined Pax3 co-labeling with markers for these cell

234   types Foxp2 and Pax2, respectively (Fujita et al., 2008; Maricich & Herrup, 1999). While

235   colocalization between Pax3 and Pax2 was found (**Figure 3B),** no co-staining between Pax3 and

236   Foxp2 was observed (**Supplemental Figure 3A**). These results extend to P0, where Pax3+ cells

237   are found in the nascent granule cell layer as well as the cerebellar parenchyma; ie co-labeling

238   with Pax2 and not Calbindin, a Purkinje cell marker (**Figure 3E, Supplemental Figure 3B**).

239   Thus, Pax3 is a novel marker for GABAergic progenitors and interneuron precursors in the

240   developing cerebellum.

241

242   **Co-expressed putative target genes are expressed in spatially distinct areas of the**

243   **developing cerebellum.**

244   We next investigated the molecular processes regulated by robust cerebellar enhancers

245   through predicting their downstream targets (Osterwalder et al., 2018; Yao et al., 2015). This was

246   done by calculating the correlation between H3K27ac signal and gene expression at E12, P0, and

247   P9 (Zhang et al., 2018) for genes located within the same conserved topological associating

248   domain (TAD) identified previously (Dixon et al., 2012) (See Methods). Overall, at least one

249   positively correlated target gene was identified for **5815/7023 (70.61%)** cerebellar enhancers

250   with an average Pearson correlation coefficient of **0.86** (Supplementary Data 3). In total, we

251   identified **2261** target genes. Using the Mouse Genome Informatics (MGI) database, we

252   identified **98** target genes that when knocked out result in a cerebellar phenotype; demonstrating

253   the validity of our high throuput approach.

254   An unbiased *k-means* clustering was then conducted for Early and Late target genes to

255   delineate them into the various co-expression programs coordinating molecular events during

256   development. For this analysis, the target gene expression time course was expanded to 12

257   different timepoints during cerebellar development, quantified previously by CAGE-seq (Zhang

258   et al., 2018). For Early active enhancers, 4 Clusters of co-expressed target genes were identified

259   (**Figure 4A**). Genes in these clusters had decreased expression over time, similar to their

260 corresponding enhancer activity. However, a distinct mean expression profile was observed for

261 each Cluster (**Figure 4B**). Interestingly, genes with known function during cerebellar

262 development showed distinct spatial expression patterns, observed using ISH data from the

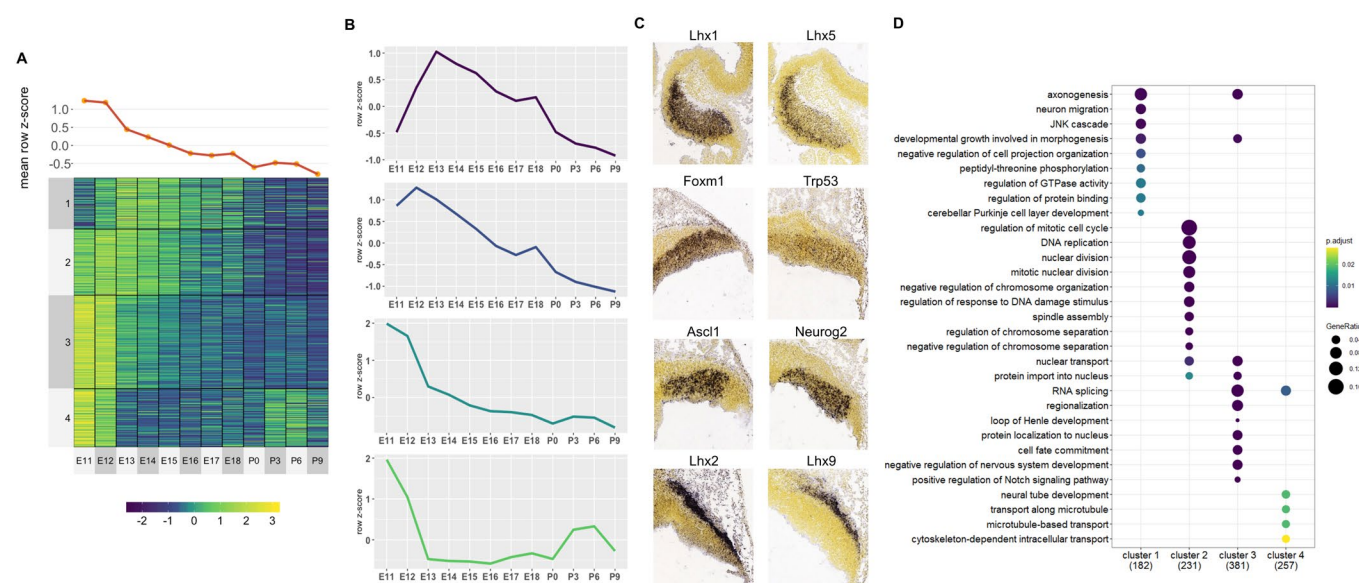263 Developing Mouse Brain Atlas (Thompson et al., 2014) (**Figure 4C**).

264

265

266 **Figure 4. Co-expressed Early target genes are expressed in spatially distinct areas and have diverse roles in**
267 **cerebellar development. A)** Line plot and heatmap showing mean z-score expression for Early target genes
268 throughout the cerebellar time course. **B)** Line graph representation of expression pattern throughout time for each
269 cluster. **C)** Known cerebellar genes in each cluster and *in situ* hybridization (ISH) images showing spatial expression
270 at peak expression ages. ISH images were taken from the Developing Mouse Atlas conducted at E13.5 for clusters 1
271 and 2, and E11.5 for clusters 3 and 4. **D)** Gene Ontology (GO) enrichment analysis of target genes from each cluster,
272 displaying the top enriched GO terms. Size of the dots indicates the gene ratio for a given cluster which is equal to
273 the number of genes within the GO category divided by the total number of genes in the cluster. Color scale
274 indicates the adjusted p-value for each GO term.

275 For example, in **Cluster 3**, cerebellar genes *Ascl1* and *Neurog2* are expressed exclusively

276 in the ventricular zone at E11.5 while **Cluster 4** contains *Lhx9* and *Meis2* which are expressed in

277 the Nuclear Transitory Zone (neurons destined for the cerebellar nuclei). A Gene Ontology (GO)

278 enrichment analysis revealed that each cluster is enriched for molecular processes known to be

279 regulated by cerebellar genes within the cluster (**Figure 4D**). For example, **Cluster 1** is enriched

280 for **axonogenesis** (GO:0007409, p-value: 3.31E-4), **neuron migration** (GO:0001764, p-value:

281 3.3E-4) and **Purkinje layer development** (GO:0021691, p-value: 0.01) and also contains *Lhx1*

282 and *Lhx5* which are expressed in migrating Purkinje cells in cerebellar parenchyma and has

283 previously been associated with the regulation of Purkinje cell differentiation during embryonic

284   cerebellar development (Zhao et al., 2007). Together, these findings support the notion that Early

285   active enhancers regulate their targets in a spatially-specific manner, regulating distinct processes

286   in their respective cell types.

287   For the Late active enhancers, 4 Clusters of co-expressed target genes were identified

288   (**Figure 5A**). We observed relatively distinct expression patterns in each of the 4 Clusters with a

289   gradual rise in mean expression throughout time **(Figure 5B)**. Genes with known function during

290   cerebellar development also show distinct spatial expression patterns, identified using the

291   Developmental Mouse Atlas (**Figure 5C**). For example, **Cluster 1** and **3** contained known

292   cerebellar genes critical for granule cell development, such as *Neurod1* and *Zic1*, while **Cluster**

293   **2** and **4** contained cerebellar genes important for in Purkinje cell development, such as *Atxn1* and

294   *Hcn1* (**Figure 5C**) (Aruga & Millen, 2018; Ebner et al., 2013; Miyata et al., 1999; Rinaldi et al., 2013).
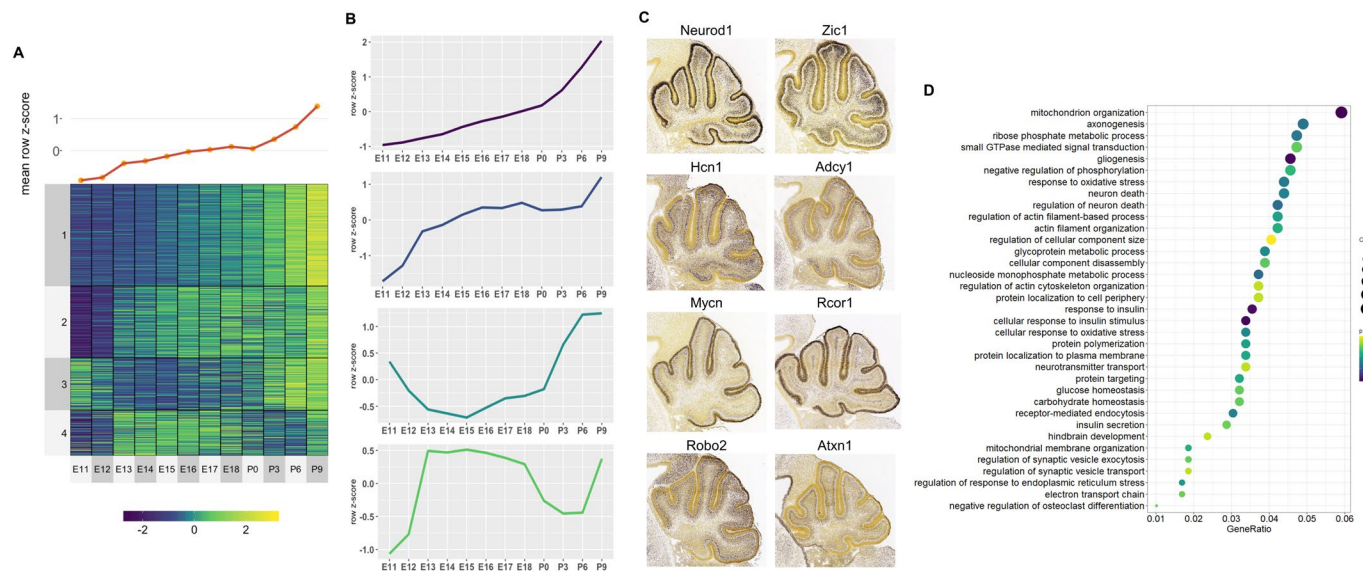

295

296   **Figure 5. Co-expressed Late target genes are expressed in developing granule cells or Purkinje cells with**
297   **common roles in cerebellar development. A)** Line plot and heatmap showing mean z-score expression throughout
298   the cerebellar time course. **B)** Line plot representation of expression pattern throughout time for each cluster. **C)**
299   Known cerebellar genes in each cluster and *in situ* hybridization showing spatial expression at peak expression ages.
300   ISH images were taken from the Developing Mouse Atlas provided by the Allen Brain Atlas conducted at P4.5 for
301   all clusters. **D)** Gene Ontology (GO) enrichment analysis of all target genes of Late active enhancers, displaying the
302   top enriched GO terms. Size of the dots indicates the number target genes within a given GO term and the gene ratio
303   (x-axis) is equal to the number of genes within the GO category divided by the total number of genes in the cluster.
304   Color scale indicates the adjusted p-value for each GO term.

305   A GO enrichment analysis was conducted for each Cluster; with no significantly

306   enriched Cluster-specific GO terms. However, if all Late enhancer target genes were combined,

307   several enriched GO terms emerged including ones involved in postnatal neuronal development,

308   such as **neuron death** (GO:0070997, p-value: 0.003), **neurotransmitter transport**

309   (GO:0006836, p-value: 0.006) and **regulation of synaptic vesicle exocytosis** (GO:2000300, p-

310   value: 0.005) (**Figure 5D**). Overall, this analysis provides a working framework for the

311   placement of hundreds of genes into the overall structure of embryonic or postnatal cerebellar

312   development

313

314   ***Bhlhe22* is a novel regulator of granule cell development**

315   To demonstrate the utility of our results, we sought to identify target genes not

316   previously identified in cerebellar development. We focused on Late Cluster 1, which contained

317   target genes expressed in granule cells. We hypothesized that genes within this cluster regulated

318   postnatal granule cell differentiation. To identify genes in this cluster regulating granule cell

319   development, we filtered these genes relative to their interaction with Atoh1, the lineage defining

320   molecule for granule cells and other glutamatergic neurons in the developing cerebellum (Ben-

321   Arie et al., 1997). The genes were filtered using the following criteria: 1) Atoh1 is bound to the

322   predicted enhancer during postnatal development (Klisch et al., 2011) and 2) the genes are

323   differentially expressed in the Atoh1-null mouse (Klisch et al., 2011). Among the top 15 genes in

324   the filtered list, we identified **4** novel genes and **11** genes that have previously been implicated in

325   postnatal granule cell development (Supplementary Table 1). The known genes provided

326   validation for our approach. The novel genes included *Bhlhe22* (also known as *Bhlhb5*), *Purb*,

327   *Klf13* and *Sox18*. We focused particularly on *Bhlhe22* as it has previously been implicated in the

328   differentiation of neurons in the cortex (Joshi et al., 2008). An enhancer ~2 kb upstream of the

329   *Bhlhe22* transcriptional start site was identified and is bound by Atoh1 during postnatal

330   development (**Supplemental Figure 3A**). This enhancer displayed H3K27ac activity highly

331   correlated (Pearson correlatoin coefficient = 0.98) to *Bhlhe22* expression, which consistently

332   rises throughout cerebellar development and peaks at P9.5 (**Supplemental Figure 3B**).

333   To attain a cellular resolution of the expression pattern for *Bhlhe22* over developmental

334   time, a time-course of protein expression using immunofluorescent staining spanning cerebellar

335   development was conducted. Bhlhe22 expression was observed in cells within the inner external
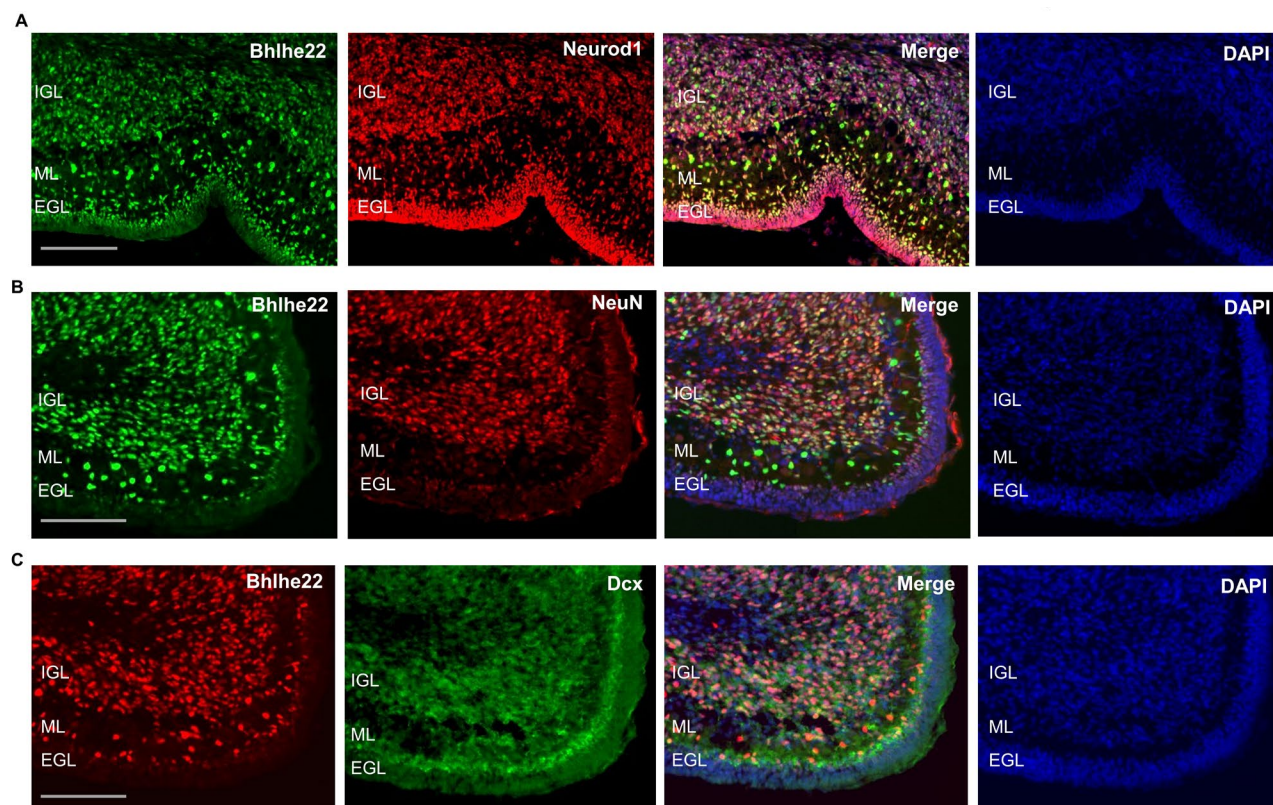
Figure 6. Bhlhe22 is expressed in differentiating granule cells in postnatal cerebellar development. A) Bhlhe22 (green) and Neurod1 (red) immunofluorescent co-staining at P9.5 of taken from a posterior lobe IX. **B)** Bhlhe22 (green) and NeuN (red) immunofluorescence co-staining at P6 taken from posterior lobe IX. **C)** Bhlhe22 (red) and Dcx (green) immunofluorescent co-staining at P6 showing the posterior lobe IX; Labels: EGL= external granular layer IGL = inner granular layer, ML = molecular layer, Scalebars = 100um.

granule layer (EGL), molecular layer and in the inner granule layer (IGL) of the postnatal

cerebellum (**Figure 6A**). To identify whether Bhlhe22 is expressed in differentiating granule

cells, co-staining experiments were performed with Neurod1 and NeuN which mark

differentiating and mature granule cells, respectively (Miyata et al., 1999; Weyer & Schilling, 2003).

At P6.5, colocalization between Bhlhe22 and Neurod1 was observed, indicating expression in

differentiating and migrating granule cells (**Figure 6A**). Co-staining between Bhlhe22 and NeuN

expression was also observed, indicating expression in maturing granule cells found within the

IGL (**Figure 6B**). To confirm whether the Bhlhe22-positive cells within the molecular layer were

migrating granule cells, we performed a double labelling experiment for a neuronal migration

marker Doublecortin (Takács, Zaninetti, Vig, Vastagh, & Hámori, 2008). Colocalization between

Doublecortin and Bhlhe22 was observed in cells within the inner EGL and the molecular layer,

confirming Bhlhe22 expression in migrating granule cells (**Figure 6C**).

355   We then investigated the role that Bhlhe22 plays in postnatal granule cell development

356   using a well-established *in vitro* system (Lee, Greene, Mason, & Manzini, 2009). Three sets of

357   experiments were performed using isolated granule cells from P6.5 cerebella transfected with

358   siRNA targeting Bhlhe22 transcripts (**Figure 7A**). First, to determine if Bhlhe22 expression was

359   diminished, changes in gene expression were assessed after 3 days *in vitro* (DIV) using reverse

360   transcriptase quantitative PCR (RT-qPCR). A 50% reduction of Bhlhe22 expression, on average,

361   was found in treated cultures compared to controls (**Figure 7B**).
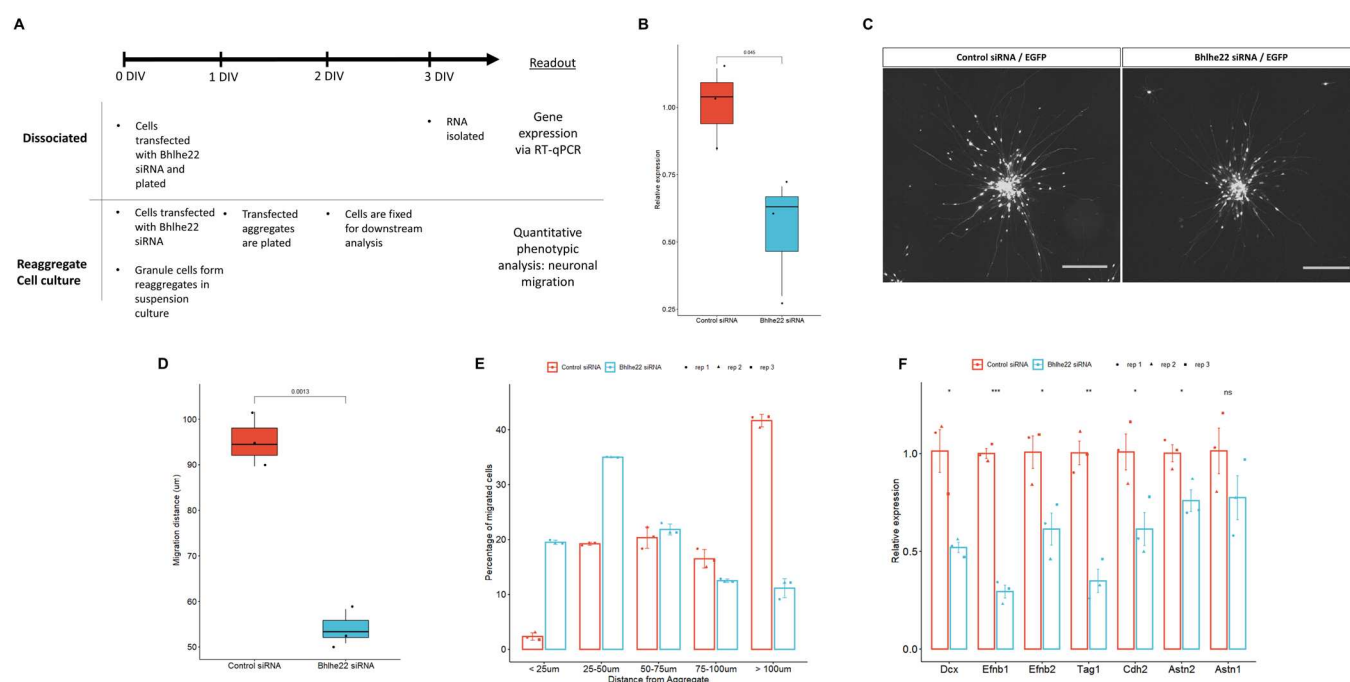

362

363   **Figure 7. Knockdown of Bhlhe22 reduces migration of cultured cerebellar granule cells. A)** Workflow for

364   dissociated and reaggregate postnatal granule cell cultures. **B)** RT-qPCR analysis of Bhlhe22 gene expression in

365   dissociated postnatal granule cell cultures after treatment with Bhlhe22 siRNA. Gene expression was normalized

366   relative to the expression of the co-transfected EGFP protein to account for transfection variability between cultures.

367   Data are presented as mean ± SD (n = 3). **C)** Image of cultured cerebellar granule cell reaggregates treated with

368   control and Bhlhe22 siRNA. Shown are EGFP positive cells indicating successful transfection. Scalebars = 100um.

369   **D)** Box plot displaying mean distance of granule cell migration from the aggregate. Value above indicates a

370   statistical difference between control cultures and those treated with Bhlhe22 siRNA (p-value = 0.0013). **E)** Bar plot

371   showing the percentage of cells migrated at different distances from the aggregate for control and Bhlhe22 siRNA

372   treated cerebellar granule cell cultures. **F)** RT-qPCR analysis of gene expression of cell adhesion molecules in

373   dissociated postnatal granule cell cultures after treatment with Bhlhe22 siRNA. Gene expression was normalized

374   relative to the expression of the co-transfected EGFP protein to account for transfection variability between cultures.

375   Data are presented as mean ± SD (n = 3). Symbols: *: $p <= 0.05$, **: $p <= 0.01$, ***: $p <= 0.001$, which indicate

376   statistical differences observed between Bhlhe22 siRNA treated samples and controls. All error bars represent the

377   standard error of the man

378

379   Second, phenotypes of the transfected cells were examined; examining their neuritic

380   outgrowths from the aggregate, and the migration of granule cells from the aggregates, within the

381   first 24 hours of plating (Gartner, Collin, & Lalli, 2006). Neuritic outgrowth was unaffected,

382   however there was a marked reduction in migration (**Figure 7C**). Bhlhe22 siRNA transfected

383   cells travelled on average 54.2um from the edge of the aggregate, a 50% reduction compared to

384   control samples (**Figure 7D**). Examining the distribution of migrated cells from the edge of the

385   aggregate, there was a higher percentage of Bhlhe22 siRNA transfected granule cells migrating

386   less than 50um, while the majority of the cells in control samples migrated 100um and beyond

387   (**Figure 7E**).

388   Third, changes in the expression of cell adhesion molecules that are known to be

389   involved in granule cell development were assessed (Consalez et al., 2021; Wang et al., 2007). A

390   significant reduction of *Efnb1, Efnb2, Tag1, Cdh2* and *Astn2* was observed in Bhlhe22

391   knockdown granule cell cultures compared to controls (**Figure 7F**). In addition to these genes,

392   we also found a significant reduction in Doublecortin (*Dcx*) expression. Taken together, these *in*

393   *vitro* knockdown experiments reveal a novel function for Bhlhe22, a gene that was identified by

394   our temporal enhancer-target gene analysis and was predicted to have a critical role in postnatal

395   granule cell development.

396

397   **Active cerebellar enhancers are enriched for common and *de novo* genetic variants**

398   **associated with autism spectrum disorder.**

399   Genome wide association studies (GWAS) have revealed that the majority of variants

400   associated with neurodevelopmental diseases are found within non-coding regulatory sequences,

401   particularly enhancers (Visel, Rubin, & Pennacchio, 2009). Given the emerging importance of the

402   cerebellum in the etiology of autism spectrum disorder (ASD), we tested whether ASD-

403   associated variants are enriched in cerebellar enhancers. The software tool GREGOR (Genomic

404   Regulatory Elements and Gwas Overlap algoRithm) was used to evaluate the enrichment of

405   common genetic variants associated with ASD in cerebellar enhancers (Schmidt et al., 2015). ASD

406   associated SNPs were retrieved from the GWAS Catalog (Buniello et al., 2019) and a stringent

407   filter was applied to identify SNPs associated with the ASD (Supplementary Table 2). We

408   examined 174 ASD-associated SNPs with a maximum p-value of 9E-06 (Buniello et al., 2019).

409   ASD-associated SNPs were enriched in cerebellar enhancers (p-value = 2.34E-03) and in

410 H3K27ac peaks at E12, P0, and P9 (p-values of 1.29E-03, 1.05E-02 and 1.42E-04, respectively)

411 (**Figure 8A**). For the 13 cerebellar enhancers containing ASD-associated SNPs, we identified 12

412 predicted target genes (Supplementary Table 3). Among these, three (*PAX6*, *TCF4*, and *ZMIZ1*)

413 are ASD risk genes according to the Simons Foundation Autism Research Initiative (SFARI)

414 gene database (Banerjee-Basu & Packer, 2010).

415   *De novo* mutations (DNMs) (variants present in the genome of a child but not his or her

416 parents) have been found to play a significant role in the etiology of ASD, including those found

417 in non-coding regions of the genome (Grove et al., 2019; Yuen et al., 2016). We hypothesized that

418 DNMs within cerebellar enhancers would be more prevalent in ASD-affected individuals

419 compared with their unaffected siblings. We used whole-genome sequencing data from 2,603

420 ASD-affected individuals and 164 unaffected siblings from the MSSNG cohort(C Yuen et al.,

421 2017), as well as 2,340 ASD-affected individuals and 1,898 unaffected siblings from the Simons

422 Simplex Collection (SSC) (Fischbach & Lord, 2010) to analyze the prevalence of DNMs in ASD-

423 affected individuals compared with their unaffected siblings.

424

A

Dataset	Reported Number of SNPs	Expected Number of SNPs	P-value
Cerebellar enhancers	13	5.31	2.34E-03
E12 H3K27ac peaks	27	15.40	1.29E-03
P0 H3K27ac peaks	5	1.37	1.05E-02
P9 H3K27ac peaks	19	7.94	1.42E-04

B

Dataset	Number of DNMs				Odds ratio (confidence interval)	P-value
	Enhancer affected	Enhancer unaffected	Non-enhancer affected	Non-enhancer unaffected		
Cerebellar enhancers	1605	609	389636	161992	1.10 (1.00, 1.21)	0.055
E12 H3K27ac peaks	4321	1726	386920	160875	1.04 (0.98, 1.10)	0.16
P0 H3K27ac peaks	337	132	390904	162469	1.06 (0.87, 1.31)	0.58
P9 H3K27ac peaks	2041	796	389200	161805	1.07 (0.98, 1.16)	0.13
Combined Coordinates	7712	3016	383529	159585	1.06 (1.02, 1.11)	0.0043

C

Enhancer Coordinates (hg38)	Predicted Target Gene	CNV Coordinates (hg38)	CNV Type	CNV Size (bp)
chr10:13928845-13929693	FAM107B	chr10:13912983-13942132	Deletion	29,150
chr11:63909702-63910591	STIP1	chr11:63907636-63910623	Deletion	2,988
chr12:96838867-96841675	NEDD1	chr12:96825001-96842000	Duplication	17,000
chr14:76714160-76716619	VASH1	chr14:76711247-76714368	Deletion	3,122
chr14:103861041-103862026	CDC42BPB	chr14:103855620-103866732	Deletion	11,113
chr15:98960270-98962257	-	chr15:98937001-99031000	Duplication	94,000
chr19:47156912-47157972	MEIS3	chr19:47133001-47184000	Duplication	51,000

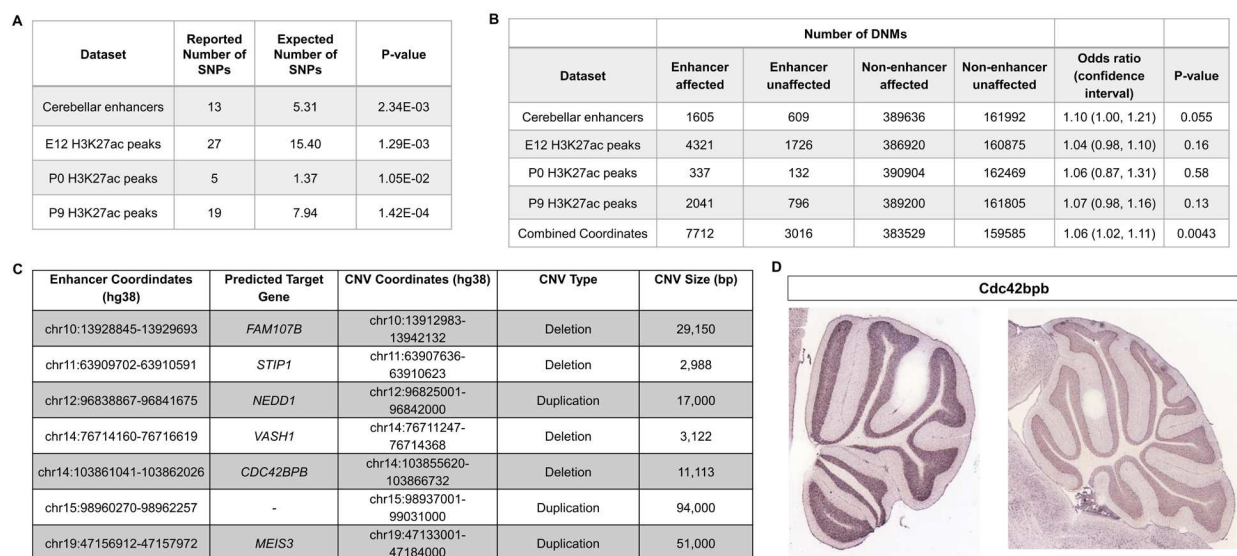**D**

Cdc42bpb

425
426
427 **Figure 8. Cerebellar enhancers are enriched for GWAS SNPs and DNMs associated with ASD. A)** Number of
428 ASD-associated GWAS variants identified in cerebellar enhancers and H3K27ac peaks called from E12, P0, and P9
429 samples. **B)** Enrichment of *de novo* single nucleotide variants and indels in ASD-affected individuals compared with
430 their unaffected siblings. Counts are not equal to the sum of the four enhancer types because some enhancers are
431 categorized as more than one type. **C)** Gene targets for enhancers overlapped by *de novo* CNVs in the SSC cohort.
432 **D)** *In situ* hybridization showing Cdc42bpb expression in the lateral (left) and medial (right) adult mouse cerebellum
433 (REF mouse brain atlas). Note expression is found in granule cells, particularly those of the lateral cerebellum.
434

435   We found that DNMs (specifically *de novo* single nucleotide variants and indels) in

436   cerebellar enhancers and H3K27ac peaks from E12, P0 and P9 were enriched in ASD-affected

437   individuals, with odds ratios ranging from 1.04 to 1.10 (**Figure 8B**). While these differences

438   were not statistically significant for cerebellar enhancers and peak coordinates individually,

439   statistical significance was achieved when combined (odds ratio=1.06; p-value=0.0043). We also

440   identified *de novo* CNVs overlapping cerebellar enhancers. Since the number of such CNVs was

441   too small to perform statistical enrichment tests, we selected a subset of 7 of these CNVs (4

442   deletions and 3 duplications) for further characterization to identify candidates for association

443   with ASD (**Figure 8C**). The most promising candidate was an ~11 kb deletion overlapping an

444   enhancer predicted to target *CDC42BPB*, which has previously been implicated in

445   neurodevelopmental phenotypes (Chilton et al., 2020). By visual validation in Integrative

446   Genomics Viewer (Robinson et al., 2011), we verified that this deletion was truly *de novo*

447   (Supplementary Figure 4**).** *CDC42BPB* is expressed in the granule cell layer of the adult mouse

448   cerebellum (**Figure 8D**) and is expressed in the lateral aspects of the cerebellum but not the

449   medial cerebellum.

450

451   **<u>Discussion</u>**

452   The current model of gene expression regulation during brain development posits that

453   temporal and spatial transcription is under the intricate control of thousands of non-coding

454   enhancer sequences (Nord & West, 2020). This model has emerged from the findings of several

455   studies of enhancer activity in various parts of the developing brain (Nord et al., 2013; Pattabiraman

456   et al., 2014; Visel et al., 2013). In our study on the cerebellum, we performed an assessment of

457   enhancer activity through genome-wide profiling of H3K4me1 and H3K27ac deposition at three

458   time points during embryonic and early postnatal times. These datasets were utilized to define

459   functional enhancer elements with temporally specific activity during these developmental ages.

460   In doing so, we establish the first catalog of predicted enhancers active during embryonic

461   cerebellum development. Through a motif enrichment analysis, neural TF motifs were found to

462   be enriched in cerebellar enhancers which may drive temporally specific enhancer activation.

463   This analysis highlighted a novel regulatory role for several understudied TFs in the context of

464   cerebellar development. These data were then integrated with a transcriptomic time course to

465   identify predicted target genes to inform our understanding of enhancer regulation in the

466 developing cerebellum. Through unbiased clustering, we identified enhancer-regulated co-

467 expression gene programs with spatially distinct patterns of expression and unique biological

468 functions during embryonic and postnatal development. Further analysis of these results led to

469 the discovery of novel cell-type marker and regulator of cerebellar development and highlights

470 the importance of enhancer regulation during brain development and the etiology of ASD.

471

472 **Cerebellar enhancers regulate gene expression important for distinct stages of neuronal**

473 **development**

474 Identification of enriched TF binding sites and putative target genes indicated that

475 cerebellar enhancers likely play a regulatory role in various phases of neuronal development. In

476 agreement with our results, previous examinations of active non-coding regulatory sequences

477 revealed that neural progenitor cells and mature neurons exhibit distinct signatures of enhancer-

478 associated histone profiles, DNA methylation, chromatin conformation and enhancer-promoter

479 interactions (Bonev et al., 2017; de la Torre-Ubieta et al., 2018; Lister et al., 2013; Whyte et al., 2012).

480 Bonev et al. (2017) examined changes in enhancer-promoter interactions between transgenic cell

481 lines FACS sorted for embryonic stem cells, neural progenitors and mature neurons and

482 identified that changes in enhancer-promoter contacts are cell-state specific and correlate with

483 changes in gene expression (Bonev et al., 2017). When comparing contacts in neuro-progenitors

484 and mature neurons, a decrease in the interaction strength was observed between active domains

485 compared to an increased strength in inactive domains, indicating a shift in usage of regulatory

486 sequences. These changes were also reflected at the level of TF binding, as interactions at Pax6-

487 bound sites, a TF marking neural progenitors, were stronger in neural progenitors than in

488 neurons, while NeuroD2-bound sites, a TF marking mature neurons, were stronger in neurons

489 than NPCs (Bonev et al., 2017). This shift in enhancer usage throughout cortical development is

490 also reflected in DNA methylation profiles, where fetal enhancers are hypermethylated and

491 decommissioned in the adult brain, while enhancers regulating adult gene expression were

492 hypomethylated (Lister et al., 2013). Hypermethylation was accompanied by a decrease in

493 H3K4me1, H3K27ac and DNase hypersensitivity while the increase was observed after

494 hypomethylation (Lister et al., 2013). Our study supports the importance of temporally-specific

495   activity during different stages of neuron development *in vivo* and details the processes driven by

496   enhancer-regulated expression during embryonic and early postnatal brain development.

497   Expression analysis of two genes novel to cerebellar development, Pax3 and Bhlhe22,

498   supported the notion that enhancer profiles are specific to developmental stage. TF enrichment

499   analysis identified Pax3 preferentially enriched in Early active enhancers and robust expression

500   of Pax3 was localized to GABAergic interneuron progenitor cells. Interestingly, through further

501   examination of cerebellar single-cell RNA-seq data produced by Carter et al. (2018), we found

502   that Pax3 expression is enriched in GABAergic progenitors and differentiating GABAergic

503   interneurons (Carter et al., 2018). Analysis of predicted gene targets of Late active enhancers

504   identified Bhlhe22 as a novel gene expressed in postnatal differentiated granule cells, and *in*

505   *vitro* knockdown experiments in primary granule cells indicated Bhlhe22 regulates granule cell

506   migration potentially through regulation of cell adhesion molecule expression. These results are

507   supported by findings in the developing cortex, where Bhlhe22 has been shown to regulate post-

508   mitotic acquisition of area identity in layers II-V of the somatosensory and caudal motor cortices

509   (Joshi et al., 2008). The contrasting expression profiles of Pax3 and Bhlhe22 highlight the wide-

510   ranging developmental impact of enhancer-mediated gene expression regulation.

511   Our findings from the TF enrichment and gene target analyses generated from

512   preferentially active postnatal enhancers indicate that many of the enhancers captured are active

513   in the developing granule cells and Purkinje cells. We attribute this apparent bias to our whole

514   tissue approach, as granule cells and Purkinje cells are the predominant cells in the cerebellum at

515   that time, making it more likely to capture signals specific to these cells compared to other less

516   abundant cell types. Our study therefore reveals that to elucidate enhancers specifically active

517   within less abundant cell types, a more granular approach may be required through single-cell

518   examination of chromatin accessibility, such as single cell ATAC-seq. This approach can be

519   coupled with the abundance of scRNA-seq data that has been collected in the developing

520   cerebellum. This strategy has seen success in the developing cortex and more recently in the

521   cerebellum (Preissl et al., 2018; Sarropoulos et al., 2021).

522

523

524 **Co-expressed gene targets of cerebellar enhancers display cell type-specific expression**
525 **patterns**

526   In addition to being temporally-specific, recent evidence indicates that enhancer activity
527 is cell type specific in the brain (Blankvoort, Witter, Noonan, Cotney, & Kentros, 2018). This is
528 highlighted in the identification of cerebellar enhancer target gene clusters for Early and Late
529 active enhancers with cell specific patterns of expression (Figure 4 and 5). For example, distinct
530 boundaries can be seen in gene expression from Early Clusters 3 and 4 at E11.5 between cells in
531 the subpial stream (Cluster 4) and neuroepithelium (Cluster 3) where neural precursors of two
532 separate lineages, the glutamatergic cerebellar nuclei and GABAergic cerebellar nuclei and
533 Purkinje cells, are found, respectively. These sharp borders are reminiscent of the small domains
534 of distinct enhancer activity identified in neural progenitors in the telencephalon, which were
535 found to fate-map to specific prefrontal cortex subdivisions (Pattabiraman et al., 2014). We see a
536 similar pattern in the more developed postnatal cerebellum, observing a spatial distinction
537 between Late Clusters 1/3 and 2/4 delineating expression in granule cells and Purkinje cells,
538 respectively. This cell type specific enhancer usage is demonstrated in the adult brain.
539 Blankvoort et al (2018) (Blankvoort et al., 2018) used ChIP-seq analysis of microdissected
540 subregions of the adult mouse cortex to reveal unique enhancer profiles pertaining to each
541 region. Additionally, Nott et al (2019) (Nott et al., 2019) identified enhancer-promoter interactome
542 maps specific to the major cell types in the cortex, which included neurons, microglia,
543 oligodendrocyte and astrocytes. Enriched GO terms for each cerebellar target gene clusters were
544 cell-type and temporally specific, highlighting enhancer specificity. Functionally annotating their
545 respective clusters provides a working hypothesis for hundreds of genes, which can be used as a
546 jumping point for future in-depth studies in the cerebellum. Collectively, these findings support
547 the notion that the cell types in the cerebellum have specific enhancer signatures relevant which
548 are reflected by the expression and functions of their target genes.

549

550 **GWAS SNPs and DNMs associated with ASD are enriched in cerebellar enhancers**

551   Having established and characterized enhancer sequences in the cerebellum, we sought to
552 elucidate the potential involvement of these regions in the etiology of neurological disorders;
553 imaging and quantitative data show consistent cerebellar abnormalities, particularly in cases of

554   individuals with autism (Limperopoulos et al., 2014) (Stoodley & Limperopoulos, 2016). Our results

555   indicate that cerebellar enhancer sequences are significantly enriched for GWAS variants and

556   DNMs associated with ASD, suggesting an important role for enhancers in contributing to the

557   condition. PAX6 was among 12 target genes of cerebellar enhancers containing ASD-associated

558   variants and is classified in the SFARI as a ASD risk gene. The deletion of Pax6 in the murine

559   cerebellum results in aberrant development of the glutamatergic cells in the cerebellum: the

560   cerebellar nuclei, unipolar brush cells and granule cells (Yeung et al., 2016). Behavioral analysis

561   of Pax6 animal models has also indicated a possible link between this gene and autistic-like

562   behavior (Umeda et al., 2010). Additionally, Pax6 has been linked with WAGR (Wilm's tumor,

563   Aniridia, Genitourinary malformations, and mental Retardation syndrome) which is co-morbid

564   for ASD. Our analysis invites future investigation these target genes and how perturbation of

565   their expression may lead to ASD phenotypes.

566   Of the target genes of the enhancers that overlapped *de novo* CNVs in the SSC cohort,

567   none have been previously associated with cerebellar development. Interestingly, one of these

568   target genes, *CDC42BPB,* has recently been associated with neurodevelopmental disorders

569   including ASD (Chilton et al., 2020). This gene is a serine/threonine protein kinase and codes for

570   MRCKβ (myotonic dystrophy-related Cdc42-binding kinase beta), a regulator of cell

571   cytoskeletal reorganization and cell migration (Pichaud, Walther, & Nunes de Almeida, 2019). Of

572   note, the CNV associated with this gene deletes the entire enhancer. CDC42BPB shows

573   expression in the granule cell layer of the lateral adult cerebellum, which has been associated

574   with cognitive functions (Koziol et al., 2014).

575   Together, our data serves as an invaluable resource for future studies, by providing

576   candidate genes involved in cerebellar development with potentially meaningful impact in the

577   etiology of ASD and other neurodevelopmental disabilities.

578

Materials and Methods

Mouse strains and husbandry

581   C57BL/6 J mice were originally purchased from JAX laboratory and maintained and bred in a

582   pathogen-free animal facility with 12/12 hour light/dark cycle and a controlled environment.

583   Embryonic ages utilized in these experiments were confirmed based upon the appearance of a

584 vaginal plug. The morning that a vaginal plug was detected was designated as E0.5. Pregnant

585 females were cervically dislocated and embryos were harvested from the uterus. Postnatal ages

586 were determined based upon the date of birth with the morning of the observation of newborn

587 pups considered as P0.5. All studies were conducted according to the protocols approved by the

588 Institutional Animal Care and Use Committee and the Canadian Council on Animal Care at the

589 University of British Columbia.

590

591 **Tissue preparation for chromatin immunoprecipitation**

592 C57BL/6 J mice (male and female) at E12.5, P0.5 and P9.5 (henceforth referred to as E12, P0,

593 and P9) were decapitated for dissection of cerebella. Cerebella were dissected and collected in

594 ice cold Dulbecco's PBS (DPBS) without magnesium or calcium and subsequently washed 2x

595 for 5 minutes. Samples from each litter were pooled and trypsinized in DPBS containing 0.25%

596 trypsin for 10, 15 and 30 min at room temperature for E12, P0 and P9, respectively. Following 3

597 washes with fresh DPBS, the tissue was triturated with 3 progressively smaller (1, 0.5, 0.1mm)

598 bore polished and sterile pipettes in DPBS containing 250U/ml DNase, 0.25% glucose, and

599 8mg/ml BSA. The triturated cells were diluted 1:4 with cold DPBS and passed through a cell

600 strainer (40μm mesh) to remove large cellular debris. The cells were collected by mild

601 centrifugation, washed in fresh DPBS and counted. The cells were split into 100,000 cell

602 aliquots, pelleted and snap frozen using liquid nitrogen. Cell pellets were stored at -80°C.

603

604 **Histone chromatin immunoprecipitation**

605 We performed native chromatin immunoprecipitation (ChIP) using validated antibodies against

606 H3K4me1 and H3K27ac according to previously established protocols by the International

607 Human Epigenomics Consortium (IHEC) (Lorzadeh, Lopez Gutierrez, Jackson, Moksa, & Hirst,

608 2017). Briefly, cells were lysed in mild non-ionic detergents (0.1% Triton X-100 and

609 Deoxycholate) and protease inhibitor cocktail (Calbiochem) to preserve the integrity of histones

610 harbouring epitopes of interest during cell lysis. Cells were digested by Microccocal nuclease

611 (MNase) at room temperature for 5 minutes and 0.25mM EDTA was used to stop the reaction.

612 Antibodies to H3K4me1 (Diagenode: Catalogue #C15410037, lot A1657D) and H3K27ac

613 (Hiroshi Kimura, Cell Biology Unit, Tokyo Institute of Technology) were incubated with anti-

614 IgA magnetic beads (Dynabeads from Invitrogen) for 2 hours. Digested chromatin was incubated

615   with magnetic beads alone for 1.5 hours. Digested chromatin was separated from the beads and

616   incubated with antibody-bead complex overnight in immunoprecipitation buffer (20mM Tris-

617   HCl pH 7.5, 2mM EDTA, 150mM NaCl, 0.1% Triton X-100, 0.1% Deoxycholate). The resulting

618   immunoprecipitations were washed 2 times by low salt (20mM Tris-HCl pH 8.0, 2mM EDTA,

619   150mM NaCl, 1% Triton X-100, 0.1% SDS) and then high salt (20mM Tris-HCl pH 8.0, 2mM

620   EDTA, 500 mM NaCl, 1% Triton X-100, 0.1% SDS) wash buffers. Immunoprecipitations were

621   eluted in an elution buffer (1% SDS, 100 mM Sodium Bicarbonate) for 1.5 hours at 65°C.

622   Remaining histones were digested by Protease (Invitrogen) for 30 minutes at 50°C and DNA

623   fragments were purified using Ampure XP beads (Beckman Coulter). The library preparation

624   was conducted by Diagenode ChIP-seq/ChIP-qPCR Profiling service (Diagenode Cat#

625   G02010000) using the MicroPlex Library Preparation Kit v2 (Diagenode Cat. C05010013). 50-

626   bp single-end sequencing was performed on all libraries by Diagenode (Belgium) on an Illumina

627   HiSeq 3000 platform. Two independent biological replicates were performed for each antibody

628   and developmental time point.

629

630   **Histone modification ChIP-seq data processing**

631   The sequencing data were uploaded to the Galaxy web platform (usegalaxy.org) for analyses

632   (Afgan et al., 2016). 50-bp single-end ChIP-seq reads were aligned to the NCBI37/mm9 reference

633   genome and converted to binary alignment/map (BAM) format by Bowtie2 v.2.3.4 (Langmead,

634   Trapnell, Pop, & Salzberg, 2009) with default parameters. Duplicate reads were marked using

635   Picard v.1.52. Peak enrichment was computed using MACS v.2.1.1 (Zhang, Y. et al., 2008) with a

636   false discovery rate (FDR) cutoff of 0.01 (p-value < 1E-5) using input samples as a control for

637   each replicate. bigWigs were generated and normalized by the total number of mapped reads

638   using the BamCompare and profiles were generated from these bigWigs by calculating average

639   coverage in 50 bp bins using Deeptools v.3.3 (Ramírez et al., 2016) for downstream analysis and

640   visualization.

641

642   **Identification of active cerebellar enhancers**

643   We first determined consensus peaks between replicates for both H3K27ac and H3K4me1 peaks

644   collected at E12, P0 and P9 using the *intersect* function from Bedtools v.2.28 (Quinlan & Hall,

645   2010). Robust active cerebellar enhancers were identified by overlapping replicated H3K27ac

646   and H3K4me1 peaks called for E12, P0 and P9 samples. The genomic coordinates of the

647   H3K27ac peaks that overlapped with H3K4me1 enriched regions at the same age were used for

648   our list of robust active cerebellar enhancers. We then removed peaks found within promoter

649   sequences by eliminating any peaks found 500bp upstream or downstream of transcription start

650   sites (TSSs) in the developing cerebellum as determined previously (Zhang et al., 2018). The

651   resulting list of robust active cerebellar enhancer sequences at E12, P0, and P9 were used for

652   downstream analysis.

653   For the comparative analysis with cerebellar postnatal enhancers previously published by Frank

654   et al. (2015), H3K27ac and DNase-seq peak coordinates were downloaded from Gene

655   Expression Omnibus (GEO) (GSE60731). The following sequences were downloaded from

656   public enhancer databases: 1) enhancers downloaded from the VISTA Enhancer Browser

657   (https://enhancer.lbl.gov/) (Visel et al., 2007) with hindbrain activity were filtered using the

658   'Advanced Search' tool, selecting "hindbrain" under Expression Pattern and retrieving only

659   mouse sequences with positive signal and 2) mouse cerebellar neonate enhancer coordinates

660   were downloaded from the Enhancer Atlas 2.0 repository

661   (http://www.enhanceratlas.org/downloadv2.php) (Gao & Qian, 2020). For the comparisons,

662   sequences were overlapped with our robust cerebellar enhancer peaks and H3K27ac peaks at

663   E12, P0 and P9 using Bedtools v.2.28(Quinlan & Hall, 2010).

664

665   **Differential binding analysis**

666   Aligned read counts (BAM file format) from our H3K27ac ChIP-seq experiments mapped to our

667   robust active cerebellar enhancers for E12, P0 and P9 samples were used as input to the package

668   DiffBind v1.4.2 (Stark & Brown, 2011). Read counting at each genomic location was conducted,

669   which was subsequently normalized by experimental input samples. The result of counting is a

670   binding affinity matrix containing normalized read counts for every sample at each robust active

671   cerebellar enhancer. For differential binding affinity analysis, three contrasts were set up in

672   DiffBind: E12 vs P0, E12 vs P9, and P0 vs P9. Differential binding was determined by DiffBind

673   using a negative binomial test at an FDR < 0.05 threshold. The FDRs and normalized signal

674   difference for each contrast were plotted using the EnhancedVolcano package in R (Kevin Blighe,

675   Sharmila Rana, & Myles Lewis, 2020).

676

Temporal classification of cerebellar enhancers

To determine cerebellar enhancers with embryonic-specific activity, H3K27ac signal at E12 was compared to P0 and P9. Enhancers with significantly higher signal at E12 for either contrast were considered "Early" active enhancers. A region found to be enriched for both contrasts was counted as one enhancer. To determine cerebellar enhancers with postnatal-specific activity, H3K27ac signal at P9 was compared to E12 and P0. Enhancers with significantly higher signal at P9 for either contrast were considered "Late" active enhancers. A region found to be enriched for both contrasts was counted as one enhancer. To determine cerebellar enhancers with activity specific to birth, H3K27ac signal at P0 was compared to P9 and E12. Enhancers with significantly higher signal at P0 in both contrasts would identify enhancers that peaked in activity at P0. We did not identify any enhancers that peaked in activity at P0 and conducted the remaining analysis for only Early and Late enhancers.

Transcription factor motif enrichment analysis

Transcription factor motif enrichment was calculated using the software HOMER using the script FindMotifsGenome.pl with default parameters (Heinz et al., 2010). Analyses for Early and Late active enhancers were conducted separately. Motif enrichment was statistically analyzed using a cumulative binomial distribution. Enriched motifs were aligned with known transcription factor binding sites to determine the best matches. Top known motif matches were filtered based on expression within the developing cerebellum at E12 for "Early" active enhancers and P9 for "Late" active enhancers.

Cerebellar enhancer target gene prediction and co-expression analysis

To identify possible gene targets of our robust cerebellar enhancers, the correlation between H3K27ac signal and mRNA expression of genes located in *cis* at E12, P0 and P9 was calculated. For a given enhancer, a gene located in *cis* was considered a possible target if it was positively correlated with H3K27ac signal throughout time. These genes were then filtered based on location using conserved topologically associating domains (TADs), which are areas of the genome that preferentially interact (Dixon et al., 2012). These TADs are conserved between different cell types and even across species and were established using Hi-C data generated, previously. Gene target candidates for a given enhancer were curated for those located within the

708   same TAD. Predicted gene targets were then ranked based on their Pearson correlation

709   coefficient value. For the predicted gene targets of Early and Late active enhancers, we

710   conducted *k-means* clustering of predicted gene targets separately. Input for this analysis was

711   gene expression captured from cerebella at 12 embryonic and postnatal time points (Zhang et al.,

712   2018). Briefly, gene expression was quantified using Cap Analysis of Gene Expression followed

713   by sequencing (CAGE-seq) for mouse cerebellar samples dissected every 24 hours from E11-P0

714   and then every 72 hours until P9 (12 in vivo time points in total). The number of clusters for the

715   *k-means* clustering was determined using the Elbow analysis for each classified group of

716   enhancers: Early (n=4) and Late (n=4).

717

Tissue preparation for histology

718

719   Embryos harvested between E11.5 to E15.5 were fixed by immersion in 4% paraformaldehyde in

720   0.1M phosphate buffer (PB, pH 7.4) for 1 hour at 4°C. Postnatal mice between P0.5 to P6.5 were

721   perfused through the heart with a saline solution followed by 4% paraformaldehyde/0.1M PBS.

722   The brain tissues were isolated and further fixed in 4% paraformaldehyde in 0.1M PB for 1 hour

723   at room temperature. Fixed tissues were rinsed with PBS, followed by cryoprotection with 30%

724   sucrose/PBS overnight at 4°C before embedding in the Optimal Cutting Temperature compound

725   (Tissue-Tek). Tissues were sectioned at 12um for immunofluorescence experiments and

726   cryosections were mounted on Superfrost slides (Thermo Fisher Scientific), air dried at room

727   temperature, and stored at −80°C until used. Sagittal sections were cut from one side of the

728   cerebellum to the other (left to right, or vice versa). In all cases, observations were based on a

729   minimum of 3 embryos per genotype per experiment.

730

Cerebellar immunostaining

731

732   Tissue sections were first rehydrated in PBS (3 x 5 minute washes) followed by a phosphate

733   buffered saline with Triton X-100 (PBS-T) rinse. Sections were then incubated at room

734   temperature for 1 hour with blocking solution (0.3% BSA, 10% normal goat serum, 0.02%

735   sodium azide in PBS-T). Following the blocking step, the slides were incubated with primary

736   antibody in incubation buffer (0.3% BSA, 5% normal goat serum, 0.02% sodium azide in PBS-

737   T) at room temperature overnight in a humid chamber. Following the overnight incubation, the

738   slides were rinsed in 3 x 10 minute PBS-T washes. The sections were then incubated with the

739 appropriate secondary antibody at room temperature for 1 hour, followed by three 0.1M PB

740 washes and one 0.01M PB wash. Coverslips were applied to the slides using FluorSave mounting

741 medium (345789, Calbiochem). The primary antibodies used were: rabbit anti-Bhlhe22 (1:1000,

742 a gift from Dr. Michael Greenburg, Harvard University), mouse anti-Neurod1 (1:500, Abcam,

743 ab60704), mouse anti-Pax3 (1:500, R&D systems, MAB2457), rabbit anti-Pax2 (1:200,

744 Invitrogen, 71-6000), mouse anti-NeuN (1:100, Millipore, MAB377), rabbit anti-Calbindin

745 (1:1000, Millipore, AB1778), rabbit anti-Foxp2 (1:2000, Novus Biologicals NB100-55411),

746 chicken anti-Doublecortin: (1:100, Abcam ab153668). For immunofluorescence, secondary

747 antibodies (Invitrogen) labeled with fluorochrome were used to recognize the primary antibodies.

748

749 **Granule cell culture**

750 Granule cells were isolated and cultured as previously described (Lee et al., 2009). Briefly,

751 cerebella from litters of P6 mice were pooled and digested at 37 °C for 20 minutes in 10U ml−1

752 papain (Worthington), and 250U ml−1 DNase in EBSS using the Papain Dissociation Kit

753 (Worthington, Cat #:LK003150). The tissue was mechanically triturated and suspended cells

754 were isolated and resuspended in EBSS with albumin-ovomucoid inhibitor solution. Cell debris

755 was removed using a discontinuous density gradient and cells were resuspended in HBSS,

756 glucose and DNase. The cell suspension was then passed through a 40um cell strainer (Falcon

757 2340), layered on a step gradient of 35% and 65% Percoll (Sigma), and centrifuged at 2,500rpm

758 for 12 minutes at 25°C. Granule cells were harvested from the 35/65% interface and washed in

759 HBSS-glucose. Granule cells were then resuspended in Neurobasal medium and 10% FBS and

760 pre-plated on lightly coated poly-D-lysine–coated dishes for 20 minutes. This step allows any

761 heavier cells to drop and adhere to the coated surface while the granule cells are retained in the

762 media. Granule cells in the media were then collected, washed and counted using a

763 Hemocytomoter. The cells were then plated on 25mm or 12mm poly-D-lysine (Sigma), laminin

764 coated coverglasses placed in 6-well plates with Neurobasal medium containing B-27 serum-free

765 supplement, 2mm l-glutamine, 100U/ml penicillin, and 100μg/ml streptomycin (pen-strep)

766 (Invitrogen, Grand Island, NY) and 0.45% d-glucose (Gibco). Granule cells were incubated at

767 37°C at 5% CO_2 were incubated for 3 days in vitro (DIV).

768 For aggregate cultures, aggregates were allowed to form by incubating purified granule cells for

769 20 hours on uncoated tissue culture dishes in DMEM containing 10% FBS, 0.45% D-glucose,

770   Pen-strep, 2mM L-glutamine at 4E6 cells/ml. Aggregates were then washed and cultured in

771   Neurobasal/B27 medium on poly-d-lysine/laminin-treated chamber slides at 37°C/5% CO2.

772   Neuronal processes extend from aggregates and most form neurite bundles. After several hours,

773   small bipolar granule cells migrate unidirectionally away from the cell clusters along these

774   neurites and neurite bundles by extension of processes, followed by translocation of cell bodies

775   outside of the aggregate cell cluster margin. For immunofluorescence experiments, cells were

776   fixed in 4% paraformaldehyde for 10 minutes and washed with calcium and magnesium-free

777   PBS.

778

779   **RNA interference**

780   For the knockdown of Bhlhe22, we purchased ON-TARGETplus SMARTPool Mouse Bhlhe22

781   siRNA from Horizon Discovery (Cat ID: L-063262-01). Control samples were transfected with

782   ON-TARGETplus Non-targeting Control Pool (Cat ID: D-001810-10). siRNA molecules were

783   electroporated into isolated postnatal cerebellar granule cells using the Nucleofector 2b Device

784   (Lonza, AAB-1001) as previously described (Gartner et al., 2006). Briefly, after cells were

785   isolated (described above), 6-7E6 cells were resuspended in nucleofection solution and mixed

786   with 3ug of pCAG-EGFP plasmid (Addgene, 89684) and 600nM of siRNA. Cuvettes were

787   loaded with cellular solution and nucleofected using program O-03. After electroporation, cells

788   were allowed to recover in DMEM media in a humidified 37°C/5% CO2 incubator for 90

789   minutes. Cells were washed and resuspended in either culture media for plating (dissociated

790   cultures) or DMEM media for overnight incubation (aggregate cultures).

791

792   **RNA isolation and reverse transcription followed by quantitative PCR (RT-qPCR)**

793   RNA was collected from cultured granule cells using the Monarch® Total RNA Miniprep Kit

794   (NEB). Then cDNA was reverse transcribed using SuperScript™ IV First-Strand Synthesis

795   System (Invitrogen) using random hexamers. Quantitative PCR was conducted using the Applied

796   Biosystems Fast SYBR Green Master Mix reagent and Applied Biosystems 7500 Real-time PCR

797   system. PCR conditions were as follows: 95 °C for 20 seconds, 40 cycles of 95 °C for 3 seconds,

798   and 60 °C for 30 seconds followed by 95 °C for 15 seconds, 60 °C for 1 minute, 95 °C for

799   15 seconds and 60 °C for 15 seconds. Three biological replicates were analyzed for each target

800   gene. Amplification of eGFP was used as a reference gene to normalize the relative amounts of

801 successfully transfected cells between treated and control experiments. Gene specific primers are

802 listed in Supplementary Table 4. Expression profiles for each gene were calculated using the

803 average relative quantity of the sample using the deltaCT method (Livak & Schmittgen, 2001). For

804 comparisons between siRNA treated and control samples, means were compared using a two-

805 tailed t-test. Results were expressed as the average ± SE, and p-values <0.05 were considered

806 significant.

807

808 **Image analysis and microscopy**

809 Analysis and photomicroscopy were performed with a Zeiss Axiovert 200M microscope with the

810 Axiocam/Axiovision hardware-software components (Carl Zeiss) and downstream image

811 analysis was conducted using the AxioVision software v.4.9.1 (Carl Zeiss). For cerebellar

812 granule cell aggregate cultures, aggregate size determined using the tracing tool and all

813 aggregates analyzed were within 1000 squared microns of each other. Transfected cells were

814 identified by examining eGFP expression and for each biological replicate/experimental

815 treatment, 20 aggregates were examined. Granule cell migration was measured by calculating the

816 distance of migrated cells from the edge of the aggregate on captured images. Mean migration

817 distance was calculated for each aggregate, and the average of all 20 aggregates was used for

818 statistical analysis. The distribution of migrated cells from the aggregate was calculated for the

819 following ranges: <25um, 25-50um, 50-75um, 75-100um, >100um. For each range, the average

820 percentage was calculated for 20 aggregates per replicate. For comparisons between siRNA

821 treated and control samples, means were compared using a two-tailed t-test. Results were

822 expressed as the average ± SE, and p-values <0.05 were considered significant.

823

824 **Plots and statistical methods**

825 All plots and correlation analysis were generated in R version 3.2.3 and figures were produced

826 using the package ggplot2. Bedtools v.2.28 (Quinlan & Hall, 2010) was used for comparing and

827 overlapping the genomic coordinates of peaks and existing genomic features described in the

828 manuscript. Boxplots represent the median (centre line), first and third quartiles (top and bottom

829 of box, respectively) and confidence intervals (95%; black lines). Genome browser screenshots

830 were taken from the IGV genome browser (Robinson et al., 2011). Bar plots results were

831 expressed as the average and the corresponding error bars represent standard error.

832

GWAS SNP enrichment analysis

Single nucleotide polymorphisms (SNPs) were retrieved from the GWAS Catalog (Buniello et al., 2019) downloaded on March 8th, 2020. The SNPs were then filtered by their associated traits. Traits containing the word "autism" were selected and from this list any traits containing the word "or" were excluded. This resulted in a final list of 8 traits (Supplementary Table 2) and the associated SNPs were used as input for our analysis. The software Genomic Regulatory Elements and Gwas Overlap algoRithm (GREGOR) v.1.4.0 (Schmidt et al., 2015), a tool to test for enrichment of an input list of trait-associated index SNPs in experimentally annotated regulatory domains, was used to identify enrichment of trait-specific disease variants within enhancers. An underlying hypothesis of GREGOR is that both trait-associated SNPs and variants in strong linkage disequilibrium (LD) may be deemed as causal. For this, we used the European population reference file (EUR; LD window size = 1 Mb; LD $r^2 \geq 0.7$) from 1000G data (Release date: May 21, 2011). The probability of an overlap of either a SNP or at least one of its LD proxies with our enhancers relative to a set of matched control variants was used to evaluate significance of overlap. The enrichment p-value is the probability that the overlap of control variants with our enhancers is greater than or equal to the overlap of the GWAS variants with our enhancers.

De novo mutation analysis

De novo mutations were detected using whole-genome sequencing data from the MSSNG (Yuen et al., 2016) and Simons Simplex Collection (SSC) (Isoda et al., 2017) cohorts using a pipeline involving DeNovoGear (Ramu et al., 2013) as previously described (C Yuen et al., 2017). To maximize data homogeneity, we included only individuals sequenced on the Illumina HiSeq X platform. Individuals having a total DNM count more than three standard deviations above the mean of the cohort were excluded. The NCBI LiftOver tool was used to convert the coordinates of cerebellar enhancers from mm9 to hg19 to hg38, and BEDTools (Quinlan & Hall, 2010) was used to identify DNMs overlapping these coordinates. Contingency tables (2x2) were generated containing counts of the number of DNMs in ASD-affected individuals and unaffected siblings either overlapping or not overlapping each dataset (cerebellar enhancer or H3K27ac peak coordinates). Fisher's exact test was used to determine statistical significance. Copy number

863 variants (CNVs) >= 1000 bp were detected from the MSSNG and SSC WGS data using a

864 pipeline involving the algorithms ERDS (Zhu et al., 2012) and CNVnator (Abyzov, Urban, Snyder,

865 & Gerstein, 2011) as previously described (Trost et al., 2018). A CNV was deemed to be *de novo* if

866 it was detected by both ERDS and CNVnator in the child but by neither algorithm in both

867 parents. We then used BEDtools (Quinlan & Hall, 2010) to identify *de novo* CNVs overlapping

868 our cerebellar enhancers.

869 **Competing Interest Statement**

870 Authors have no competing interests.

871

872 **Author Contributions**

873 M.R. conducted experiments and was responsible for all major areas of concept formation, data

874 collection, analysis and manuscript composition. Y.B. processed and analyzed ChIP-seq data and

875 conducted the human variant enrichment analysis as well as contributed to manuscript writing.

876 J.Y. was involved in all mouse breeding and sample collection. J.W. and E.Y. were involved in

877 the initial profiling of Pax3 and conducting immunofluorescent experiments. B.T. and S.W.S.

878 conducted all genome-wide sequencing and analysis for the enrichment of autism spectrum

879 disorder variants. D.G. was the supervisory author and was involved in all areas of concept

880 formation and manuscript edits. All authors contributed to the final drafting of the manuscript.

881

882 **References**

883 Abyzov, A., Urban, A. E., Snyder, M., & Gerstein, M. (2011). CNVnator: An approach to

884 discover, genotype, and characterize typical and atypical CNVs from family and population

885 genome sequencing. *Genome Research, 21*(6), 974-984. doi:10.1101/gr.114876.110

886 Afgan, E., Baker, D., van den Beek, M., Blankenberg, D., Bouvier, D., Čech, M., . . . Goecks, J.

887 (2016). The galaxy platform for accessible, reproducible and collaborative biomedical

888 analyses: 2016 update. *Nucleic Acids Research, 44*(W1), W3-W10. doi:10.1093/nar/gkw343

889 Aruga, J., & Millen, K. J. (2018). ZIC1 function in normal cerebellar development and human

890 developmental pathology. *Advances in Experimental Medicine and Biology, 1046*, 249-268.

891 doi:10.1007/978-981-10-7311-3_13

892 Banerjee-Basu, S., & Packer, A. (2010). SFARI gene: An evolving database for the autism

893 research community. *Disease Models & Mechanisms, 3*(3-4), 133-135.

894 doi:10.1242/dmm.005439

895 Barešić, A., Nash, A. J., Dahoun, T., Howes, O., & Lenhard, B. (2020). Understanding the

896 genetics of neuropsychiatric disorders: The potential role of genomic regulatory blocks.

897 *Molecular Psychiatry, 25*(1), 6-18. doi:10.1038/s41380-019-0518-x

898   Ben-Arie, N., Bellen, H. J., Armstrong, D. L., McCall, A. E., Gordadze, P. R., Guo, Q., . . .
899   Zoghbi, H. Y. (1997). Math1 is essential for genesis of cerebellar granule neurons. *Nature,*
900   *390*(6656), 169-172. doi:10.1038/36579

901   Blankvoort, S., Witter, M. P., Noonan, J., Cotney, J., & Kentros, C. (2018). Marked diversity of
902   unique cortical enhancers enables neuron-specific tools by enhancer-driven gene expression.
903   *Current Biology: CB, 28*(13), 2103-2114.e5. doi:10.1016/j.cub.2018.05.015

904   Bonev, B., Mendelson Cohen, N., Szabo, Q., Fritsch, L., Papadopoulos, G. L., Lubling, Y., . . .
905   Cavalli, G. (2017). Multiscale 3D genome rewiring during mouse neural development. *Cell,*
906   *171*(3), 557-572.e24. doi:10.1016/j.cell.2017.09.043

907   Buniello, A., MacArthur, J. A. L., Cerezo, M., Harris, L. W., Hayhurst, J., Malangone, C., . . .
908   Parkinson, H. (2019). The NHGRI-EBI GWAS catalog of published genome-wide
909   association studies, targeted arrays and summary statistics 2019. *Nucleic Acids Research,*
910   *47*(D1), D1005-D1012. doi:10.1093/nar/gky1120 [doi]

911   C Yuen, R. K., Merico, D., Bookman, M., L Howe, J., Thiruvahindrapuram, B., Patel, R. V., . . .
912   Scherer, S. W. (2017). Whole genome sequencing resource identifies 18 new candidate
913   genes for autism spectrum disorder. *Nature Neuroscience, 20*(4), 602-611.
914   doi:10.1038/nn.4524

915   Calo, E., & Wysocka, J. (2013). Modification of enhancer chromatin: What, how, and why?
916   *Molecular Cell, 49*(5), 825-837. doi:10.1016/j.molcel.2013.01.038

917   Carter, R. A., Bihannic, L., Rosencrance, C., Hadley, J. L., Tong, Y., Phoenix, T. N., . . . Gawad,
918   C. (2018). A single-cell transcriptional atlas of the developing murine cerebellum. *Current*
919   *Biology: CB, 28*(18), 2910-2920.e2. doi:10.1016/j.cub.2018.07.062

920   Carullo, N. V. N., & Day, J. J. (2019). Genomic enhancers in brain health and disease. *Genes,*
921   *10*(1) doi:10.3390/genes10010043

922   Chilton, I., Okur, V., Vitiello, G., Selicorni, A., Mariani, M., Goldenberg, A., . . . Chung, W. K.
923   (2020). De novo heterozygous missense and loss-of-function variants in CDC42BPB are
924   associated with a neurodevelopmental phenotype. *American Journal of Medical Genetics.*
925   *Part A, 182*(5), 962-973. doi:10.1002/ajmg.a.61505

926   Consalez, G. G., Goldowitz, D., Casoni, F., & Hawkes, R. (2021). Origins, development, and
927   compartmentation of the granule cells of the cerebellum. *Frontiers in Neural Circuits, 14*
928   doi:10.3389/fncir.2020.611841

929   Creyghton, M. P., Cheng, A. W., Welstead, G. G., Kooistra, T., Carey, B. W., Steine, E. J., . . .
930   Jaenisch, R. (2010). Histone H3K27ac separates active from poised enhancers and predicts
931   developmental state. *Proceedings of the National Academy of Sciences of the United States*
932   *of America, 107*(50), 21931-21936. doi:10.1073/pnas.1016071107

de la Torre-Ubieta, L., Stein, J. L., Won, H., Opland, C. K., Liang, D., Lu, D., & Geschwind, D. H. (2018). The dynamic landscape of open chromatin during human cortical neurogenesis. *Cell, 172*(1-2), 289-304.e18. doi:10.1016/j.cell.2017.12.014

Dixon, J. R., Selvaraj, S., Yue, F., Kim, A., Li, Y., Shen, Y., . . . Ren, B. (2012). Topological domains in mammalian genomes identified by analysis of chromatin interactions. *Nature, 485*(7398), 376-380. doi:10.1038/nature11082

Ebner, B. A., Ingram, M. A., Barnes, J. A., Duvick, L. A., Frisch, J. L., Clark, H. B., . . . Orr, H. T. (2013). Purkinje cell ataxin-1 modulates climbing fiber synaptic input in developing and adult mouse cerebellum. *The Journal of Neuroscience: The Official Journal of the Society for Neuroscience, 33*(13), 5806-5820. doi:10.1523/JNEUROSCI.6311-11.2013

Elsen, G. E., Bedogni, F., Hodge, R. D., Bammler, T. K., MacDonald, J. W., Lindtner, S., . . . Hevner, R. F. (2018). The epigenetic factor landscape of developing neocortex is regulated by transcription factors Pax6→ Tbr2→ Tbr1. *Frontiers in Neuroscience, 12*, 571. doi:10.3389/fnins.2018.00571

Fischbach, G. D., & Lord, C. (2010). The simons simplex collection: A resource for identification of autism genetic risk factors. *Neuron, 68*(2), 192-195. doi:10.1016/j.neuron.2010.10.006

Frank, C. L., Liu, F., Wijayatunge, R., Song, L., Biegler, M. T., Yang, M. G., . . . West, A. E. (2015). Regulation of chromatin accessibility and zic binding at enhancers in the developing cerebellum. *Nature Neuroscience, 18*(5), 647-656. doi:10.1038/nn.3995

Frantz, G. D., Bohner, A. P., Akers, R. M., & McConnell, S. K. (1994). Regulation of the POU domain gene SCIP during cerebral cortical development. *The Journal of Neuroscience: The Official Journal of the Society for Neuroscience, 14*(2), 472-485.

Fujita, E., Tanabe, Y., Shiota, A., Ueda, M., Suwa, K., Momoi, M. Y., & Momoi, T. (2008). Ultrasonic vocalization impairment of Foxp2 (R552H) knockin mice related to speech-language disorder and abnormality of purkinje cells. *Proceedings of the National Academy of Sciences of the United States of America, 105*(8), 3117-3122. doi:10.1073/pnas.0712298105

Gao, T., & Qian, J. (2020). EnhancerAtlas 2.0: An updated resource with enhancer annotation in 586 tissue/cell types across nine species. *Nucleic Acids Research, 48*(D1), D58-D64. doi:10.1093/nar/gkz980 [doi]

Gartner, A., Collin, L., & Lalli, G. (2006). Nucleofection of primary neurons. *Methods in Enzymology, 406*, 374-388. doi:S0076-6879(06)06027-7 [pii]

Goldowitz, D., & Hamre, K. (1998). The cells and molecules that make a cerebellum. *Trends in Neurosciences, 21*(9), 375-382.

968 Grove, J., Ripke, S., Als, T. D., Mattheisen, M., Walters, R. K., Won, H., . . . Børglum, A. D.
969 (2019). Identification of common genetic risk variants for autism spectrum disorder. *Nature*
970 *Genetics, 51*(3), 431-444. doi:10.1038/s41588-019-0344-8

971 Heinz, S., Benner, C., Spann, N., Bertolino, E., Lin, Y. C., Laslo, P., . . . Glass, C. K. (2010).
972 Simple combinations of lineage-determining transcription factors prime cis-regulatory
973 elements required for macrophage and B cell identities. *Molecular Cell, 38*(4), 576-589.
974 doi:10.1016/j.molcel.2010.05.004 [doi]

975 Heinz, S., Romanoski, C. E., Benner, C., & Glass, C. K. (2015). The selection and function of
976 cell type-specific enhancers. *Nature Reviews. Molecular Cell Biology, 16*(3), 144-154.
977 doi:10.1038/nrm3949

978 Hoshino, M., Nakamura, S., Mori, K., Kawauchi, T., Terao, M., Nishimura, Y. V., . . .
979 Nabeshima, Y. (2005). Ptf1a, a bHLH transcriptional gene, defines GABAergic neuronal
980 fates in cerebellum. *Neuron, 47*(2), 201-213. doi:10.1016/j.neuron.2005.06.007

981 Isoda, T., Moore, A. J., He, Z., Chandra, V., Aida, M., Denholtz, M., . . . Murre, C. (2017). Non-
982 coding transcription instructs chromatin folding and compartmentalization to dictate
983 enhancer-promoter communication and T cell fate. *Cell, 171*(1), 103-119.e18.
984 doi:10.1016/j.cell.2017.09.001

985 Joshi, P. S., Molyneaux, B. J., Feng, L., Xie, X., Macklis, J. D., & Gan, L. (2008). Bhlhb5
986 regulates the postmitotic acquisition of area identities in layers II-V of the developing
987 neocortex. *Neuron, 60*(2), 258-272. doi:10.1016/j.neuron.2008.08.006

988 Kevin Blighe, Sharmila Rana, & Myles Lewis. (2020). EnhancedVolcano: Publication-ready
989 volcano plots with enhanced colouring and labeling [computer software]

990 Kim, E. J., Battiste, J., Nakagawa, Y., & Johnson, J. E. (2008). Ascl1 (Mash1) lineage cells
991 contribute to discrete cell populations in CNS architecture. *Molecular and Cellular*
992 *Neurosciences, 38*(4), 595-606. doi:10.1016/j.mcn.2008.05.008 [doi]

993 Klisch, T. J., Xi, Y., Flora, A., Wang, L., Li, W., & Zoghbi, H. Y. (2011). In vivo Atoh1
994 targetome reveals how a proneural transcription factor regulates cerebellar development.
995 *Proceedings of the National Academy of Sciences, 108*(8), 3288-3293.

996 Koziol, L. F., Budding, D., Andreasen, N., D'Arrigo, S., Bulgheroni, S., Imamizu, H., . . .
997 Yamazaki, T. (2014). Consensus paper: The cerebellum's role in movement and cognition.
998 *Cerebellum (London, England), 13*(1), 151-177. doi:10.1007/s12311-013-0511-x

999 Langmead, B., Trapnell, C., Pop, M., & Salzberg, S. L. (2009). Ultrafast and memory-efficient
1000 alignment of short DNA sequences to the human genome. *Genome Biology, 10*(3), R25.
1001 doi:10.1186/gb-2009-10-3-r25

1002   Lee, H. Y., Greene, L. A., Mason, C. A., & Manzini, M. C. (2009). Isolation and culture of post-
1003   natal mouse cerebellar granule neuron progenitor cells and neurons. *Journal of Visualized*
1004   *Experiments : JoVE, (23). pii: 990. doi*(23), 10.3791/990. doi:10.3791/990 [doi]

1005   Leto, K., Bartolini, A., Yanagawa, Y., Obata, K., Magrassi, L., Schilling, K., & Rossi, F. (2009).
1006   Laminar fate and phenotype specification of cerebellar GABAergic interneurons. *The*
1007   *Journal of Neuroscience: The Official Journal of the Society for Neuroscience, 29*(21),
1008   7079-7091. doi:10.1523/JNEUROSCI.0957-09.2009

1009   Leto, K., Carletti, B., Williams, I. M., Magrassi, L., & Rossi, F. (2006). Different types of
1010   cerebellar GABAergic interneurons originate from a common pool of multipotent progenitor
1011   cells. *The Journal of Neuroscience: The Official Journal of the Society for Neuroscience,*
1012   *26*(45), 11682-11694. doi:10.1523/JNEUROSCI.3656-06.2006

1013   Limperopoulos, C., Chilingaryan, G., Sullivan, N., Guizard, N., Robertson, R. L., & du Plessis,
1014   A. J. (2014). Injury to the premature cerebellum: Outcome is related to remote cortical
1015   development. *Cerebral Cortex (New York, N.Y.: 1991), 24*(3), 728-736.
1016   doi:10.1093/cercor/bhs354

1017   Lindtner, S., Catta-Preta, R., Tian, H., Su-Feher, L., Price, J. D., Dickel, D. E., . . . Rubenstein, J.
1018   L. R. (2019). Genomic resolution of DLX-orchestrated transcriptional circuits driving
1019   development of forebrain GABAergic neurons. *Cell Reports, 28*(8), 2048-2063.e8.
1020   doi:10.1016/j.celrep.2019.07.022

1021   Lister, R., Mukamel, E. A., Nery, J. R., Urich, M., Puddifoot, C. A., Johnson, N. D., . . . Ecker, J.
1022   R. (2013). Global epigenomic reconfiguration during mammalian brain development.
1023   *Science (New York, N.Y.), 341*(6146), 1237905. doi:10.1126/science.1237905

1024   Livak, K. J., & Schmittgen, T. D. (2001). Analysis of relative gene expression data using real-
1025   time quantitative PCR and the 2(-delta delta C(T)) method. *Methods (San Diego, Calif.),*
1026   *25*(4), 402-408. doi:10.1006/meth.2001.1262 [doi]

1027   Lorzadeh, A., Lopez Gutierrez, R., Jackson, L., Moksa, M., & Hirst, M. (2017). Generation of
1028   native chromatin immunoprecipitation sequencing libraries for nucleosome density analysis.
1029   *Journal of Visualized Experiments : JoVE, (130). doi*(130), 10.3791/56085.
1030   doi:10.3791/56085 [doi]

1031   Maricich, S. M., & Herrup, K. (1999). Pax-2 expression defines a subset of GABAergic
1032   interneurons and their precursors in the developing murine cerebellum. *Journal of*
1033   *Neurobiology, 41*(2), 281-294. doi:10.1002/(sici)1097-4695(19991105)41:23.0.co;2-5

1034   Miyata, T., Maeda, T., & Lee, J. E. (1999). NeuroD is required for differentiation of the granule
1035   cells in the cerebellum and hippocampus. *Genes & Development, 13*(13), 1647-1652.
1036   doi:10.1101/gad.13.13.1647

1037 Nord, A. S., Blow, M. J., Attanasio, C., Akiyama, J. A., Holt, A., Hosseini, R., . . . Visel, A.
1038   (2013). Rapid and pervasive changes in genome-wide enhancer usage during mammalian
1039   development. *Cell, 155*(7), 1521-1531. doi:10.1016/j.cell.2013.11.033

1040 Nord, A. S., & West, A. E. (2020). Neurobiological functions of transcriptional enhancers.
1041   *Nature Neuroscience, 23*(1), 5-14. doi:10.1038/s41593-019-0538-5

1042 Nott, A., Holtman, I. R., Coufal, N. G., Schlachetzki, J. C. M., Yu, M., Hu, R., . . . Glass, C. K.
1043   (2019). Brain cell type-specific enhancer-promoter interactome maps and disease-risk
1044   association. *Science (New York, N.Y.), 366*(6469), 1134-1139. doi:10.1126/science.aay0793

1045 Osterwalder, M., Barozzi, I., Tissières, V., Fukuda-Yuzawa, Y., Mannion, B. J., Afzal, S. Y., . . .
1046   Pennacchio, L. A. (2018). Enhancer redundancy provides phenotypic robustness in
1047   mammalian development. *Nature, 554*(7691), 239-243. doi:10.1038/nature25461

1048 Pattabiraman, K., Golonzhka, O., Lindtner, S., Nord, A. S., Taher, L., Hoch, R., . . . Rubenstein,
1049   J. L. R. (2014). Transcriptional regulation of enhancers active in protodomains of the
1050   developing cerebral cortex. *Neuron, 82*(5), 989-1003. doi:10.1016/j.neuron.2014.04.014

1051 Peng, J., Sheng, A., Xiao, Q., Shen, L., Ju, X., Zhang, M., . . . Luo, Z. (2019). Single-cell
1052   transcriptomes reveal molecular specializations of neuronal cell types in the developing
1053   cerebellum. *Journal of Molecular Cell Biology,* doi:10.1093/jmcb/mjy089

1054 Pichaud, F., Walther, R. F., & Nunes de Almeida, F. (2019). Regulation of Cdc42 and its
1055   effectors in epithelial morphogenesis. *Journal of Cell Science, 132*(10)
1056   doi:10.1242/jcs.217869

1057 Porter, F. D., Drago, J., Xu, Y., Cheema, S. S., Wassif, C., Huang, S. P., . . . Westphal, H.
1058   (1997). Lhx2, a LIM homeobox gene, is required for eye, forebrain, and definitive
1059   erythrocyte development. *Development (Cambridge, England), 124*(15), 2935-2944.

1060 Preissl, S., Fang, R., Huang, H., Zhao, Y., Raviram, R., Gorkin, D. U., . . . Ren, B. (2018).
1061   Single-nucleus analysis of accessible chromatin in developing mouse forebrain reveals cell-
1062   type-specific transcriptional regulation. *Nature Neuroscience, 21*(3), 432-439.
1063   doi:10.1038/s41593-018-0079-3

1064 Quinlan, A. R., & Hall, I. M. (2010). BEDTools: A flexible suite of utilities for comparing
1065   genomic features. *Bioinformatics (Oxford, England), 26*(6), 841-842.
1066   doi:10.1093/bioinformatics/btq033

1067 Ramírez, F., Ryan, D. P., Grüning, B., Bhardwaj, V., Kilpert, F., Richter, A. S., . . . Manke, T.
1068   (2016). deepTools2: A next generation web server for deep-sequencing data analysis.
1069   *Nucleic Acids Research, 44*(W1), 160. doi:10.1093/nar/gkw257

1070   Ramu, A., Noordam, M. J., Schwartz, R. S., Wuster, A., Hurles, M. E., Cartwright, R. A., &
1071   Conrad, D. F. (2013). DeNovoGear: De novo indel and point mutation discovery and
1072   phasing. *Nature Methods, 10*(10), 985-987. doi:10.1038/nmeth.2611

1073   Rinaldi, A., Defterali, C., Mialot, A., Garden, D. L. F., Beraneck, M., & Nolan, M. F. (2013).
1074   HCN1 channels in cerebellar purkinje cells promote late stages of learning and constrain
1075   synaptic inhibition. *The Journal of Physiology, 591*(22), 5691-5709.
1076   doi:10.1113/jphysiol.2013.259499

1077   Robinson, J. T., Thorvaldsdottir, H., Winckler, W., Guttman, M., Lander, E. S., Getz, G., &
1078   Mesirov JP, -. e. (2011). Integrative genomics viewer. *Nature Biotechnology, 29*(1), 24-26.
1079   doi:10.1038/nbt.1754 [doi]

1080   Sanchez-Ortiz, E., Cho, W., Nazarenko, I., Mo, W., Chen, J., & Parada, L. F. (2014). NF1
1081   regulation of RAS/ERK signaling is required for appropriate granule neuron progenitor
1082   expansion and migration in cerebellar development. *Genes & Development, 28*(21), 2407-
1083   2420. doi:10.1101/gad.246603.114

1084   Sarropoulos, I., Sepp, M., Frömel, R., Leiss, K., Trost, N., Leushkin, E., . . . Kaessmann, H.
1085   (2021). The regulatory landscape of cells in the developing mouse cerebellum. *bioRxiv,* ,
1086   2021.01.29.428632. doi:10.1101/2021.01.29.428632

1087   Schmidt, E. M., Zhang, J., Zhou, W., Chen, J., Mohlke, K. L., Chen, Y. E., & Willer, C. J.
1088   (2015). GREGOR: Evaluating global enrichment of trait-associated variants in epigenomic
1089   features using a systematic, data-driven approach. *Bioinformatics (Oxford, England),*
1090   *31*(16), 2601-2606. doi:10.1093/bioinformatics/btv201 [doi]

1091   Stark, R., & Brown, G. (2011). DiffBind: Differential binding analysis of ChIP-seq peak
1092   data.[computer software]

1093   Stoodley, C. J., & Limperopoulos, C. (2016). Structure-function relationships in the developing
1094   cerebellum: Evidence from early-life cerebellar injury and neurodevelopmental disorders.
1095   *Seminars in Fetal & Neonatal Medicine, 21*(5), 356-364. doi:10.1016/j.siny.2016.04.010

1096   Su, X., Liu, X., Ni, L., Shi, W., Zhu, H., Shi, J., . . . Huang, Q. (2016). GFAP expression is
1097   regulated by Pax3 in brain glioma stem cells. *Oncology Reports, 36*(3), 1277-1284.
1098   doi:10.3892/or.2016.4917

1099   Swanson, D. J., & Goldowitz, D. (2011). Experimental sey mouse chimeras reveal the
1100   developmental deficiencies of Pax6-null granule cells in the postnatal cerebellum.
1101   *Developmental Biology, 351*(1), 1-12. doi:10.1016/j.ydbio.2010.11.018

1102   Takács, J., Zaninetti, R., Vig, J., Vastagh, C., & Hámori, J. (2008). Postnatal expression of
1103   doublecortin (dcx) in the developing cerebellar cortex of mouse. *Acta Biologica Hungarica,*
1104   *59*(2), 147-161. doi:10.1556/ABiol.59.2008.2.2

1105   Thompson, C. L., Ng, L., Menon, V., Martinez, S., Lee, C., Glattfelder, K., . . . Jones, A. R.
1106   (2014). A high-resolution spatiotemporal atlas of gene expression of the developing mouse
1107   brain. *Neuron, 83*(2), 309-323. doi:10.1016/j.neuron.2014.05.033

1108   Trost, B., Walker, S., Wang, Z., Thiruvahindrapuram, B., MacDonald, J. R., Sung, W. W. L., . . .
1109   Scherer, S. W. (2018). A comprehensive workflow for read depth-based identification of
1110   copy-number variation from whole-genome sequence data. *American Journal of Human
1111   Genetics, 102*(1), 142-155. doi:10.1016/j.ajhg.2017.12.007

1112   Umeda, T., Takashima, N., Nakagawa, R., Maekawa, M., Ikegami, S., Yoshikawa, T., . . .
1113   Osumi, N. (2010). Evaluation of Pax6 mutant rat as a model for autism. *PloS One, 5*(12),
1114   e15500. doi:10.1371/journal.pone.0015500

1115   Urbánek, P., Fetka, I., Meisler, M. H., & Busslinger, M. (1997). Cooperation of Pax2 and Pax5
1116   in midbrain and cerebellum development. *Proceedings of the National Academy of Sciences
1117   of the United States of America, 94*(11), 5703-5708. doi:10.1073/pnas.94.11.5703

1118   Visel, A., Minovitsky, S., Dubchak, I., & Pennacchio, L. A. (2007). VISTA enhancer browser--a
1119   database of tissue-specific human enhancers. *Nucleic Acids Research, 35*(Database issue),
1120   88. doi:10.1093/nar/gkl822

1121   Visel, A., Rubin, E. M., & Pennacchio, L. A. (2009). Genomic views of distant-acting enhancers.
1122   *Nature, 461*(7261), 199-205. doi:10.1038/nature08451

1123   Visel, A., Taher, L., Girgis, H., May, D., Golonzhka, O., Hoch, R. V., . . . Rubenstein, J. L. R.
1124   (2013). A high-resolution enhancer atlas of the developing telencephalon. *Cell, 152*(4), 895-
1125   908. doi:10.1016/j.cell.2012.12.041

1126   Wang, V. Y., & Zoghbi, H. Y. (2001). Genetic regulation of cerebellar development. *Nature
1127   Reviews. Neuroscience, 2*(7), 484-491. doi:10.1038/35081558

1128   Wang, W., Mullikin-Kilpatrick, D., Crandall, J. E., Gronostajski, R. M., Litwack, E. D., &
1129   Kilpatrick, D. L. (2007). Nuclear factor I coordinates multiple phases of cerebellar granule
1130   cell development via regulation of cell adhesion molecules. *Journal of Neuroscience,
1131   27*(23), 6115-6127.

1132   Weyer, A., & Schilling, K. (2003). Developmental and cell type-specific expression of the
1133   neuronal marker NeuN in the murine cerebellum. *Journal of Neuroscience Research, 73*(3),
1134   400-409. doi:10.1002/jnr.10655

1135   Whyte, W. A., Bilodeau, S., Orlando, D. A., Hoke, H. A., Frampton, G. M., Foster, C. T., . . .
1136   Young, R. A. (2012). Enhancer decommissioning by LSD1 during embryonic stem cell
1137   differentiation. *Nature, 482*(7384), 221-225. doi:10.1038/nature10805

1138   Wizeman, J. W., Guo, Q., Wilion, E. M., & Li, J. Y. (2019). Specification of diverse cell types
1139   during early neurogenesis of the mouse cerebellum. *eLife, 8* doi:10.7554/eLife.42388

1140   Yao, P., Lin, P., Gokoolparsadh, A., Assareh, A., Thang, M. W., & Voineagu, I. (2015).
1141   Coexpression networks identify brain region-specific enhancer RNAs in the human brain.
1142   *Nature Neuroscience, 18*(8), 1168-1174. doi:10.1038/nn.4063 [doi]

1143   Yeung, J., Ha, T. J., Swanson, D. J., & Goldowitz, D. (2016a). A novel and multivalent role of
1144   Pax6 in cerebellar development. *The Journal of Neuroscience: The Official Journal of the*
1145   *Society for Neuroscience, 36*(35), 9057-9069. doi:10.1523/JNEUROSCI.4385-15.2016

1146   Yeung, J., Ha, T. J., Swanson, D. J., & Goldowitz, D. (2016b). A novel and multivalent role of
1147   Pax6 in cerebellar development. *The Journal of Neuroscience: The Official Journal of the*
1148   *Society for Neuroscience, 36*(35), 9057-9069. doi:10.1523/JNEUROSCI.4385-15.2016

1149   Yuen, R. K. C., Merico, D., Cao, H., Pellecchia, G., Alipanahi, B., Thiruvahindrapuram, B., . . .
1150   Scherer, S. W. (2016). Genome-wide characteristics of de novo mutations in autism. *NPJ*
1151   *Genomic Medicine, 1*, 160271-1602710. doi:10.1038/npjgenmed.2016.27

1152   Zhang, D., Stumpo, D. J., Graves, J. P., DeGraff, L. M., Grissom, S. F., Collins, J. B., . . .
1153   Blackshear, P. J. (2006). Identification of potential target genes for RFX4_v3, a
1154   transcription factor critical for brain development. *Journal of Neurochemistry, 98*(3), 860-
1155   875. doi:10.1111/j.1471-4159.2006.03930.x

1156   Zhang, P. G. Y., Yeung, J., Gupta, I., Ramirez, M., Ha, T., Swanson, D. J., . . . Goldowitz, D.
1157   (2018). Discovery of transcription factors novel to mouse cerebellar granule cell
1158   development through laser-capture microdissection. *Cerebellum (London, England),*
1159   doi:10.1007/s12311-017-0912-3

1160   Zhang, Y., Liu, T., Meyer, C. A., Eeckhoute, J., Johnson, D. S., Bernstein, B. E., . . . Liu, X. S.
1161   (2008). Model-based analysis of ChIP-seq (MACS). *Genome Biology, 9*(9), R137.
1162   doi:10.1186/gb-2008-9-9-r137

1163   Zhao, Y., Kwan, K., Mailloux, C. M., Lee, W., Grinberg, A., Wurst, W., . . . Westphal, H.
1164   (2007). LIM-homeodomain proteins Lhx1 and Lhx5, and their cofactor Ldb1, control
1165   purkinje cell differentiation in the developing cerebellum. *Proceedings of the National*
1166   *Academy of Sciences of the United States of America, 104*(32), 13182-13186.
1167   doi:10.1073/pnas.0705464104

1168   Zhu, M., Need, A. C., Han, Y., Ge, D., Maia, J. M., Zhu, Q., . . . Goldstein, D. B. (2012). Using
1169   ERDS to infer copy-number variants in high-coverage genomes. *American Journal of*
1170   *Human Genetics, 91*(3), 408-421. doi:10.1016/j.ajhg.2012.07.004

1171   Ziats, M. N., Grosvenor, L. P., & Rennert, O. M. (2015). Functional genomics of human brain
1172   development and implications for autism spectrum disorders. *Translational Psychiatry, 5*,
1173   e665. doi:10.1038/tp.2015.153